

# **BRNO UNIVERSITY OF TECHNOLOGY**

VYSOKÉ UČENÍ TECHNICKÉ V BRNĚ

## **FACULTY OF MECHANICAL ENGINEERING**

FAKULTA STROJNÍHO INŽENÝRSTVÍ

## **INSTITUTE OF MATERIALS SCIENCE AND ENGINEERING**

ÚSTAV MATERIÁLOVÝCH VĚD A INŽENÝRSTVÍ

# **EFFECT OF HEAT TREATMENTS ON THE MICROSTRUCTURE AND HARDNESS OF HIGH-ENTROPY ALLOY**

VLIV TEPELNÉHO ZPRACOVÁNÍ NA MIKROSTRUKTURU A TVRDOST SLITINY S VYSOKOU ENTROPIÍ

### **BACHELOR'S THESIS**

BAKALÁŘSKÁ PRÁCE

### **AUTHOR**

AUTOR PRÁCE

**Mária Ľudmila Jesenská**

### **SUPERVISOR**

VEDOUĆÍ PRÁCE

**Larissa Moravčíková de Almeida Gouvêa**

**BRNO 2021**

# Assignment Bachelor's Thesis

Institut: Institute of Materials Science and Engineering  
Student: **Mária Ludmila Jesenská**  
Degree program: Applied Sciences in Engineering  
Branch: Materials Engineering  
Supervisor: **Larissa Moravčíková de Almeida Gouvêa**  
Academic year: 2020/21

As provided for by the Act No. 111/98 Coll. on higher education institutions and the BUT Study and Examination Regulations, the director of the Institute hereby assigns the following topic of Bachelor's Thesis:

## **Effect of heat treatments on the microstructure and hardness of high-entropy alloy**

### **Brief Description:**

High-entropy alloys, also known as complex concentrated alloys, emerged as a new class of metals that consist of three to five elements in near-equiatomic ratios. These alloys have captivated the attention of the scientific community in the last fifteen years, as some of them were proven to exhibit very interesting combinations of properties. Due to the significantly broad range of compositional space of the high entropy alloys, many compositions were not studied thoroughly up to date, therefore prospecting an ample range of opportunities for scientific research yet to be explored.

The  $\text{Al}_{0.2}\text{Co}_{1.5}\text{CrFeNi}_{1.5}\text{Ti}$  high entropy alloy and its variants have stood out as potential real alternatives for applications in which high wear resistance is required, due to their excellent wear resistance combined with high strength. Despite the very interesting properties, these alloys possess low ductility due to their complex microstructure.

In this light, this bachelor thesis aims to investigate the effect of heat treatment processes on the microstructural evolution and hardness of the  $\text{Al}_{0.2}\text{Co}_{1.5}\text{CrFeNi}_{1.5}\text{Ti}$  alloy. The annealing conditions will be chosen according to the calculated phase diagrams using ThermoCalc software and a detailed comparison of the states will be performed in terms of microstructural features, chemical composition of the phases, and hardness. During the work, the student will get to know the processes of heat treatment and microstructural analysis (SEM).

**Bachelor's Thesis goals:**

- Microstructural characterization of the cast high-entropy alloy by means of SEM, EDS.
- Computation of the respective phase diagram by ThermoCalc software.
- Analysis of the annealing influence on the properties of the material by a throughout comparison of these samples with the as-cast state.
- Hardness evaluation of all states.

**Recommended bibliography:**

MURTY, B. S., J. W. YEH and S. RANGANATHAN. High-Entropy Alloys, Elsevier, Butterworth-Heinemann, London, 2014.

MIRACLE, D. B. and O. N. SENKOV. A critical review of high entropy alloys and related concepts. Acta Materialia [online]. 2017, 122, 448-511. DOI: 10.1016/j.actamat.2016.08.081. ISSN 1359-6454. Dostupné z: <https://www.sciencedirect.com/science/article/pii/S1359645416306759>

GORSSE, S., MIRACLE, D. B. and O. N. SENKOV. Mapping the world of complex concentrated alloys. Acta Materialia [online]. 2017, 135, 177-187. DOI: 10.1016/j.actamat.2017.06.027. ISSN 1359-6454. Dostupné z: <https://www.sciencedirect.com/science/article/pii/S1359645417305025>

Deadline for submission Bachelor's Thesis is given by the Schedule of the Academic year 2020/21

In Brno,

L. S.

---

prof. Ing. Ivo Dlouhý, CSc.  
Director of the Institute

---

doc. Ing. Jaroslav Katolický, Ph.D.  
FME dean

## **Abstract**

In this work, a non-equiatomic  $\text{Al}_{0.2}\text{Co}_{1.5}\text{CrFeNi}_{1.5}\text{Ti}$  high entropy alloy was produced through the vacuum induction melting process. The as-cast alloy was analyzed, then heat treated at  $1000\text{ }^\circ\text{C}$  for 5h, and subsequent heat treatment at  $750\text{ }^\circ\text{C}$  for an additional 5h took place, in order to investigate the effect of heat treatment temperature and time on the phase composition, microstructure, and mechanical properties of the alloy in all states. A pseudo binary phase diagram (CALPHAD) was performed to evaluate the possible phases present in the alloy. The alloy's microstructures were characterized and analyzed chemically by X-ray diffraction (XRD), scanning electron microscopy (SEM), and energy dispersive spectroscopy (EDS). Microhardness and nanoindentation testing was performed to evaluate the hardness of the material.

## **Keywords**

high entropy alloy, characterization, heat treatment, microstructure, chemical composition, hardness

## **Abstrakt**

V tejto práci je študovaná neekviatomická  $\text{Al}_{0.2}\text{Co}_{1.5}\text{CrFeNi}_{1.5}\text{Ti}$  vysoko entropická zliatina, ktorá bola vyrobená pomocou vákuového indukčného tavenia. Zliatina v odliatom stave bola analyzovaná a tepelne spracovaná pri teplote  $1000\text{ }^\circ\text{C}$  po dobu 5h, a následne podrobená tepelnému spracovaniu pri teplote  $750\text{ }^\circ\text{C}$  po dobu ďalších 5h, s cieľom skúmania vplyvu teploty a doby tepelného spracovania na fázové zloženie, mikroštruktúru a mechanické vlastnosti. Na vyhodnotenie možných fáz prítomných v zliatine bol použitý pseudobinárny fázový diagram (CALPHAD). Mikroštruktúra zliatin bola charakterizovaná a chemicky analyzovaná pomocou röntgenovej difrakcie (XRD), elektrónovej mikroskopie (SEM) a energeticky disperznej spektroskopie. Výsledné vyhodnotenie tvrdosti materiálu prebehlo pomocou skúšok mikrotvrdosti a nanoindentácie.

## **Kľúčové slová**

zliatina s vysokou entropiou, charakterizácia, tepelné spracovanie, mikroštruktúra, chemické zloženie, tvrdosť

## Rozšírený abstrakt

Vysoko entropické zliatiny predstavujú nový koncept vývoja konštrukčných materiálov, ktorý je založený na zmiešaní piatich a viacerých prvkov v približne rovnakých atomárnych pomeroch. Za posledných 17 rokov priťahujú čoraz väčšiu pozornosť, kvôli jedinečnému zloženiu a vysokému potenciálu.

Prvá zmienka o vysoko entropických zliatinách, pochádza z konca 18. storočia, kedy nemecký chemik Franz Karl Achard pripravil sériu zliatin, ktoré sa skladali z piatich až siedmich hlavných prvkov s rovnakým atomárnym pomerom. Bohužiaľ, táto pozoruhodná štúdia z oblasti materiálov bola od metalurgov a vedcov z celého sveta väčšinou ignorovaná a zabudnutá. A to až do roku 1963, kedy si túto prácu všimol britský metalurg, Cyril Stanley Smith.

Koncept zliatin s rovnakým atomárnym pomerom prvkov bol popísaný až v 90 rokoch 20. storočia, kedy prof. Brian Cantor na Universty of Cambridge a prof. Jien-Wei Yeh na National Tsing Hua University začali skúmať ekvatomické zliatiny takmer v rovnakom čase a nezávisle na sebe. Navrhli nový koncept konštrukčných zliatin, ktoré obsahovali viacero hlavných prvkov a boli charakterizované vysokou konfiguračnou entropiou miešania. Domnievali sa, že ak je konfiguračná entropia miešania viacerých prvkov v rovnakom pomere dostatočne vysoká na to, aby prevládla nad entalpiou vzniku zlúčenín, tak by to viedlo k stabilizácii jednoduchých/dvojitých fáz tuhého roztoku. Preto sa táto nová trieda materiálov nazýva vysoko entropické zliatiny, aj keď v literatúre sa príležitostne používajú alternatívne názvy ako „multi-principal element alloys“ a „compositionally complex alloys“. Nedávno sa však ukázalo, že táto myšlienka neplatí pre väčšinu vysoko entropických zliatin. Aj keď vysoko entropické zliatiny boli najprv definované ako zliatiny, ktoré sa skladajú z piatich alebo viacerých hlavných prvkov, pričom koncentrácia každého hlavného prvku je približne v rozmedzí od 5-35 at. %, nedávno sa tento koncept rozšíril aj na zliatiny s tromi (stredne entropické zliatiny) alebo štyrmi hlavnými prvkami.

Vysoko entropické zliatiny možno pripravovať pomocou niekoľkých metód, ktoré je možné rozdeliť na odlievanie z taveniny, mechanické legovanie a práškovú metalurgiu. Aby sa mohla zabezpečiť vyššia konfiguračná energia zliatiny, tak každý prvok z ktorého sa zliatina skladá si musí zachovať vyššiu koncentráciu. Z tohto dôvodu, je v procese prípravy vysoko entropických zliatin zásadnou otázkou, ako legovať rôzne kovové prvky s rôznymi vlastnosťami, štruktúrou a teplotami tavenia, aby sa vytvorili homogénne zliatiny a bola zachovaná vysoká konfiguračná entropia systému. Pri výbere vhodného výrobného postupu vysoko entropických zliatin je potrebné zohľadniť morfológiu a mikroštruktúru daného systému.

V dôsledku rozdielneho chemického zloženia, vysoko entropické zliatiny vykazujú vynikajúce vlastnosti ako je pevnosť, ťažnosť a mimoriadna odolnosť voči opotrebeniu, korózii a oxidácii. Z vyššie uvedeného dôvodu sú vysoko entropické zliatiny zaradené medzi pokročilú triedu materiálov s aplikačným potenciálom v rôznych priemyselných odvetviach. Okrem toho bolo vydaných viacero štúdií, ktoré dokazujú že fázové zloženie, mikroštruktúra a výsledné vlastnosti môžu byť ovplyvnené tepelným spracovaním, tak ako v tradičných systémoch.

Experimentálna časť bakalárskej práce, sa zoberá štúdiom fázového zloženia, mikroštruktúry a mechanických vlastností vysoko entropickej zliatiny v odliatom stave a v stave po tepelnom spracovaní. Vysoko entropická zliatina  $\text{Al}_{0.2}\text{Co}_{1.5}\text{CrFeNi}_{1.5}\text{Ti}$ , bola podrobená tepelnému spracovaniu pri teplote  $1000\text{ }^\circ\text{C}$  po dobu 5h, a následne pri teplote  $750\text{ }^\circ\text{C}$  po dobu ďalších 5h.

Experimenty tepelného spracovania boli uskutočnené so zámerom zlepšenia mechanických vlastností, ktoré je možné dosiahnuť znížením obsahu intermetalických fáz prítomných v zliatine. Na vyhodnotenie možných fáz v zliatine bol použitý výpočet pseudobinárneho fázového diagramu metódou CALPHAD s využitím programu ThermoCalc. Okrem toho sa experimentálna časť uskutočnila pomocou röntgenovej difrakcie (XRD), skenovacej elektrónovej mikroskopie (SEM) a analýz energetickej disperznej spektroskopie (EDS). Tieto experimentálne metódy boli použité pre odhalenie fáz, mikroštruktúr, chemického zloženia a kryštalografických vlastností  $\text{Al}_{0.2}\text{Co}_{1.5}\text{CrFeNi}_{1.5}\text{Ti}$  HEA v stave odliatom a v stave po tepelnom spracovaní. Hodnotenie mechanických vlastností súvisiacich s rôznymi mikroštruktúrami zliatin, bolo charakterizované meraním tvrdosti materiálu pomocou mikroindentačných a nanoindentačných skúšok.

Z vyššie uvedených experimentov, je možné vyvodit' nasledujúce závery: priemerné chemické zloženie pre  $\text{Al}_{0.2}\text{Co}_{1.5}\text{CrFeNi}_{1.5}\text{Ti}$  HEA v odliatom stave, určeného pomocou analýzy EDS, zodpovedá požadovanému teoretickému zloženiu, pre  $\text{Al}_{0.2}\text{Co}_{1.5}\text{CrFeNi}_{1.5}\text{Ti}$  HEA vyrobenú pomocou vákuového indukčného tavenia.

Výsledky röntgenovej difrakcie potvrdili rovnaké fázové zloženie u  $\text{Al}_{0.2}\text{Co}_{1.5}\text{CrFeNi}_{1.5}\text{Ti}$  HEA, ktorá bola tepelne spracovaná pri teplote  $1000\text{ }^\circ\text{C}$  po dobu 5h, a následne tepelne spracovaná pri teplote  $750\text{ }^\circ\text{C}$  po dobu ďalších 5h, ako bolo predpokladané ThermoCalc simuláciou. Naopak,  $\text{Al}_{0.2}\text{Co}_{1.5}\text{CrFeNi}_{1.5}\text{Ti}$  HEA, ktorá bola tepelne spracovaná pri teplote  $1000\text{ }^\circ\text{C}$  po dobu 5h, sa mala skladať podľa ThermoCalc-u len z tuhých roztokov FCC a BCC, ale podľa röntgenovej difrakcie obsahovala fázy FCC, BCC, Lavesovu fázu a tiež sigma fázu. V oboch prípadoch tepelne spracovaných zliatin bola potvrdená aj prítomnosť novej hexagonálnej fázy  $\text{D}_{024}$ , ktorá sa vylúčila počas ochladzovania. Hexagonálna fáza  $\text{D}_{024}$  nebola zistená v odliatom stave. Na to, aby bolo možné potvrdiť prítomnosť fáz v zliatine, ktoré boli predpovedané simuláciou ThermoCalc, je potrebná optimalizácia teploty a času.

Nárast mikrotvrdosti na hodnotu  $751\pm 49\text{ HV}_{0.2}$ , bol pozorovaný v tepelne spracovanej  $\text{Al}_{0.2}\text{Co}_{1.5}\text{CrFeNi}_{1.5}\text{Ti}$  HEA pri teplote  $1000\text{ }^\circ\text{C}$  po dobu 5h s následným tepelným spracovaním pri teplote  $750\text{ }^\circ\text{C}$  po dobu ďalších 5h v porovnaní s tepelne spracovanou  $\text{Al}_{0.2}\text{Co}_{1.5}\text{CrFeNi}_{1.5}\text{Ti}$  HEA pri teplote  $1000\text{ }^\circ\text{C}$  po dobu 5h, ktorá dosahovala hodnotu mikrotvrdosti  $606\pm 47\text{ HV}_{0.2}$ . Tento nárast mikrotvrdosti je možné vysvetliť vyšším obsahom intermetalických fáz v  $\text{Al}_{0.2}\text{Co}_{1.5}\text{CrFeNi}_{1.5}\text{Ti}$  HEA, ktorá bola tepelne spracovaná pri teplote  $1000\text{ }^\circ\text{C}$  po dobu 5h s následným tepelným spracovaním pri teplote  $750\text{ }^\circ\text{C}$  po dobu ďalších 5h, ako bolo predpokladané ThermoCalc simuláciou.

Hodnoty nanoindentácie  $\text{Al}_{0.2}\text{Co}_{1.5}\text{CrFeNi}_{1.5}\text{Ti}$  HEA v odliatom stave, pre dendritickú a interdendritickú oblasť dosahovali výrazne odlišné hodnoty. Pre dendritickú oblasť nanotvrdosť dosahovala hodnoty  $7234\pm 380\text{ MPa}$  a pre interdendritickú oblasť  $11760\pm 1089\text{ MPa}$ . Vyššiu hodnotu nanotvrdosti v interdendritických regiónoch možno

vysvetliť zvýšenou prítomnosťou intermetalických sigma a Lavesových fáz v  $\text{Al}_{0.2}\text{Co}_{1.5}\text{CrFeNi}_{1.5}\text{Ti}$  HEA. Výsledné hodnoty modulu pružnosti v ťahu, pre  $\text{Al}_{0.2}\text{Co}_{1.5}\text{CrFeNi}_{1.5}\text{Ti}$  HEA v odliatom stave vypočítaného pomocou metódy Oliver-Pharr, ktoré boli podobné v rámci svojej štandardnej odchýlky, dosahovali pre dendritickú oblasť približne  $221 \pm 11$  GPa a pre interdendritickú oblasť  $223 \pm 50$  GPa.

## **Bibliographic citation**

JESENSKÁ, Mária Ludmila. *Effect of heat treatments on the microstructure and hardness of high-entropy alloy*. Brno: Vysoké učení technické v Brně, Fakulta strojního inženýrství, 2021. 42 s. Vedoucí bakalářské práce Ing. Larissa Moravčíková de Almeida Gouvêa.

## **Declaration**

I hereby declare that I am the sole author of the written work here enclosed and that I have compiled it in my own words. The work was made under the supervision of Ing. Larissa Moravčíková de Almeida Gouvêa.

Brno.....

.....  
Mária Ľ. Jesenská

## **Acknowledgments**

My greatest gratitude and appreciation goes to my supervisor Ing. Larissa Moravčíková de Almeida Gouvêa. I want to thank her for her support, patience, critical comments, and suggestion. I would like to thank doc. Ing. Antonín Záděra, Ph.D., and his team, for providing the casting of the material presented in this study. I would also like to thank my parents for the love and support they gave me over these three years. Finally, I would like to thank my boyfriend, for the motivation he has given me over the last two years.

## Table of contents

1	Introduction .....	1
2	High Entropy Alloys .....	2
2.1	History .....	2
2.2	Definition.....	3
2.3	Four ,, 'core effects' “ .....	5
2.4	Preparation and Processing.....	9
2.5	Microstructures of High Entropy Alloys .....	11
2.6	General Properties .....	14
3	Aim of the work .....	17
4	Experimental material and methods .....	18
4.1	Experimental material preparation .....	18
4.2	Characterization methods .....	19
5	Results and discussion.....	21
5.1	Calculation of phase diagrams - CALPHAD .....	21
5.2	XRD analysis .....	22
5.3	Microstructure evaluation.....	24
5.4	EDS analysis.....	28
5.5	Microhardness and nanoindentation hardness evaluation .....	32
6	Conclusions .....	35
	Bibliography.....	36
	List of abbreviations.....	42

# 1 Introduction

High entropy alloys (HEAs) as a new class of metallic materials, first proposed in 1995 by Yeh [1], are based on mixing at least five principal elements in equal or near-equal ratio, which the concentration of each element may be between 5-35 at. %. This concept is in contrast to the traditional approach based on one principal element. Common metallurgy knowledge based on binary/ternary phase diagrams suggests that the higher number of elements in multicomponent systems, the more likely it is that several types of phases and intermetallic compounds will form. However, Yeh et al. [2], believed that if the configurational entropy of mixing of several elements in the same ratio is high enough to predominate over the enthalpy of compound formation, thereby it could stabilize single/double phases of solid solution. Recently, though, this concept has been shown to not be true for most HEAs. Therefore, this new class of materials has been called high entropy alloys, although alternative names such as multi-principal element alloys and compositionally complex alloys are occasionally used in the literature [3].

Although, HEAs were first defined as alloys consisting of five or more major elements, the HEAs concept has recently been extended to include alloys with three (medium entropy alloys) or four principal elements as well [3-5]. Nowadays, most of the reported HEAs are usually prepared by vacuum induction melting technology. However, the shape and size of final products produced by vacuum induction melting are limited, and the cost of HEAs can be much higher than most common alloys, due to the inclusion of more expensive elements [6].

Due to the variation in elemental chemistry, HEAs exhibits excellent properties in a wide range of fields, such as hard strength and ductility [5, 7], exceptional wear [8], corrosion [9], and oxidation [10] resistance. Therefore, HEAs have been presented as a promising advanced class of materials with huge potential uses in various industries. In addition, there have been many studies, which have proved that the microstructure and properties of many HEAs can be changed by heat treatment [11]. Niu et al. [12] studied the annealing of  $Al_{0.5}CoCrFeNi$  HEA at 650 °C and found that the nano-sized B2 phase appeared in the dendrite region, which enhanced the strength of the alloy. Similar results were also found in the study of Xu et al. [13].

In order to investigate the effect of heat treatment temperature on the microstructure and mechanical properties of the  $Al_{0.2}Co_{1.5}CrFeNi_{1.5}Ti$  high entropy alloy, the HEA samples were heat-treated at 1000 °C for 5h with subsequent 750 °C for an additional 5h. The microstructure evolution and mechanical properties of as-cast and heat-treated samples were thoroughly discussed.

## 2 High Entropy Alloys

High entropy alloys, also known as complex concentrated alloys, emerged as a new class of material that consists of three to five elements in near equiatomic ratios. These alloys have captivated the attention of the scientific community in the last fifteen years due to their potential to be developed for real applications. In this light, the history, definition, main concepts, and most remarkable properties are introduced.

### 2.1 History

The first mention of multicomponent equimass alloys comes from the end of the 18th century. The first one who studied multi principal-element alloys with five or seven elements was a German scientist and metallurgist Karl Franz Achard. In some way, he is a predecessor of both Jien Wie Yeh's and Brian Cantor's discoveries and researches on high entropy alloys. All his work was ignored until the year 1963 when professor Cyril Stanley Smith brought it to light [14].

Two independent publications in 2004 by prof. Jien-Wei Yeh in Taiwan and prof. Brian Cantor in the United Kingdom led to start-up research on the barely touched high entropy alloy's world [2]. This nomenclature was not used previously, but the concept was similar to the ones presented already, at the end of the 18th century. In 1981, Brian Cantor with his student Alain Vincet tried to create equiatomic alloys, these consisted of alloys comprising different elements in the same atomic ratio [15]. It was found by them that one specific alloy manufactured by induction melting with CrMnFeCoNi composition, known up to now as the famous Cantor Alloy forms a single cubic centered solid solution (FCC). In 1998 the same alloy was produced using melt spinning technology, but a publication on these experiments was not published until 2004 [16].

However, a decade later Otto, F. et al. [17] discovered that Cantor alloy dissolves into metallic (BCC-Cr) and intermetallic (L10-NiMn and B2-FeCo) phases after heat treatments above 800°C. Some of these transformations appear very quickly when the alloy is in the nanocrystalline form but takes longer in large-grained materials. It is not known whether this diversity is due to the grain barrier allowing favorable nucleation location or/and rapid diffusion paths. After heat treatments above 800 °C, the metastable FCC, solid-solution state can be preserved at room temperature at normal cooling rates. These findings and others reported in the literature, contradict the first idea that high entropy alloys favor the formation of single phase solid solutions. This concept will be discussed in detail in the definition section. The microstructure has been observed by the authors at various length scales using XRD, scanning electron microscopy, transmission electron microscopy (TEM), electron backscatter diffraction, and atom probe tomography [18]. The alloy exhibited a single-phase, FCC, solid solution without visible grouping or arranging in short distances. If by chance local ordering was experimentally proven to exist, results from density functional theory calculations suggest that it would have a high impact on the stacking-fault energy and dislocation mobility, which

have a major effect on mechanical properties control [19]. At low temperatures, below 50 K, the calculations result from experimental DFT exhibit transformation of unstable FCC structure into HCP structure [20]. However, it has never been proven directly by experiments [21].

Jien Wie-Yeh started his analysis of multicomponent alloys in 1995. His idea was that a high mixing entropy factor could reduce the content of phases and change valuable properties. With his student K.H. Huang, in 1996, they prepared around 40 equiatomic alloys with five to nine elements (Ti, V, Cr, Fe, Co, Ni, Cu, Mo, Zr, Pd, and Al) by arc melting. The microstructure, corrosion resistance, and hardness were examined in an as-cast state and in a fully annealed state in these alloys. From the experimental results was evaluated that typical dendritic structure was visible in the as-cast state structure. All these observed alloys have a high hardness level in the range from 590 to 890 HV, depending on if it is in an as-cast state or fully annealed state, among with excellent corrosion resistance in four acids solutions (HCl, H<sub>2</sub>SO<sub>4</sub>, HNO<sub>3</sub>, and HF). In the year 2004, the first Jien's HEA concept paper was submitted and published in the *Advanced Engineering Materials* journal. The term HEAs was not used in any of these articles [14, 22].

Nowadays, the concept of HEAs represents a category of alloys, which provides us unique compositions, microstructures, and various properties. From recent articles, we know that not all HEAs form a solid solution, so research is also involved in the probability of the formation of a solid solution based on the difference in atomic sizes of used elements [23]. The biggest disadvantage is that there is currently no thermodynamic and kinetic evidence that represents the HEAs system [24].

On the other hand, future research of HEAs systems is expected to show promising chemical, mechanical and physical properties. This is in response to increasing requirements in material science, for the improvement of already existing materials [25].

## 2.2 Definition

### *Definition based on the composition*

In recent years, there has been some controversy about the definitions of HEAs, that are accepted in the field of science. The first definition was proposed from initial research based on compositional requirements. The HEAs are defined as alloys that consist of five or more major elements in the same or similar atomic ratio, where the concentration of major elements can vary between 5-35 atomic percentages. Also, the alloy can be enriched with additive elements to improve its properties, where the atomic percentage usually does not exceed more than 5.

This definition can be expressed by using the following equation:

$$n_{\text{major}} \geq 5, 5 \text{ at. \%} \leq c_i \leq 35 \text{ at. \%} \quad (1)$$

$$n_{\text{minor}} \geq 0, c_j \leq 5 \text{ at. \%} \quad (2)$$

, where  $n_{\text{major}}$  is a number of primary elements,  $n_{\text{minor}}$  is a number of secondary elements,  $c_i$  is atomic percentages of primary elements and  $c_j$  is atomic percentages of secondary elements.

As defined above, an alloy system with assumed high entropy may be composed of an equimolar ratio, a plurality of non-equimolar elements, or a plurality of minor elements. The definition was believed to express the probability of solid solution formation being increased with entropy [26]. However, it describes HEAs only in terms of their composition but does not explain the size of their entropy [27].

### ***Definition based on the entropy***

The standard definition of HEAs, as revealed by many researchers contains at least five major or principal elements that have an atomic concentration between 5 and 35 percent. In particular, it indicates that the stability of the disordered solution was found to be very high with a respect to the perfectly ordered intermetallic compound when the alloys have a high mixing entropy ( $\Delta S_{\text{mix}}$ ). According to the hypothesis of Boltzmann, it defines the entropy of alloys as a linear function of the logarithm which can be explained by the following equation:

$$S = k \cdot \ln W \quad (3)$$

, where  $S$  is the entropy of the system ( $\text{J}\cdot\text{K}^{-1}$ ), the value of  $k=1.38 \times 10^{-23} \text{ J/K}$  is a constant know as Boltzmann constant ( $\text{J}\cdot\text{K}^{-1}$ ) and  $W$  is the thermodynamic probability, which represents the total number of microscopic states contained in the macroscopic state.

The most suitable way for calculating the entropy of alloys composed of two elements with an atomic fraction of  $x_1$  and  $x_2$  is using Stirling's approximation as an expression:

$$S_{\text{mix}} = -k (x_1 \ln x_1 + x_2 \ln x_2) \quad (4)$$

If the ideal entropy configuration of the alloys is equal to  $n$  we can modify it as:

$$S_{\text{mix}} = -R \sum x_i \ln(x_i) \quad (5)$$

, where  $1 \leq i \leq n$  and  $R$  is a gas constant.

Because they have the same atomic fraction ( $x_i = 1/n$ ), the above equation is reduced to:

$$S_{\text{mix}} = R \ln(n) \quad (6)$$

, where  $n$  is a concentration of mixing elements in an equimolar ratio.

It is a valuable equation that works for liquid alloys, as well as for many solid high entropy alloys close to melting temperature. In equimolar HEAs,  $\Delta S_{\text{mix}}$  was firstly calculated to be  $1.61R$ . For non-equiatomic HEAs, the value of  $\Delta S_{\text{mix}}$  can be very lower  $1.5R$ . Conventional alloys have  $\Delta S_{\text{mix}}$  values arrange from  $0.22 R$  for low alloy steel and lift up to  $1.15R$  for stainless steel. Superalloys have entropy values range up to  $1.37 R$ . Low entropy is defined as  $\Delta S_{\text{mix}} \leq R$ , for medium entropy alloys  $R \leq \Delta S_{\text{mix}} \leq 1.5R$  and for high entropy, alloy  $\Delta S_{\text{mix}} \geq R$  [23].

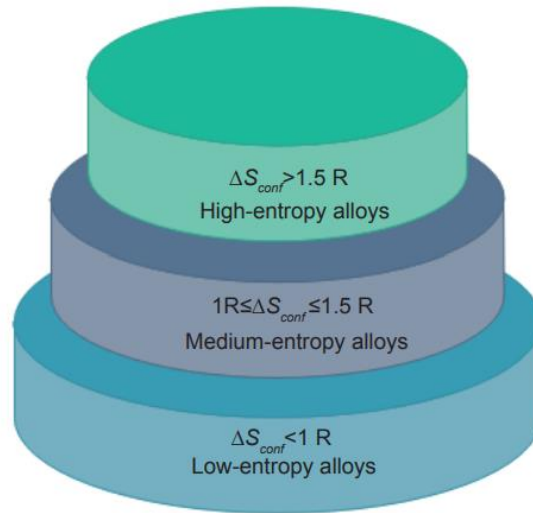


**Fig. 1** Classification of alloy based on the configurational entropy [48].

However, the above formula does not take into account vibrational entropy, magnetic entropy, and electronic randomness entropy due to the dominance of configurational entropy [28]. These are contributions that were recently proven to have a huge influence on the final properties and structures of these alloys, therefore a single value of entropy of mixing does not indicate if the alloy will stabilize solid solution phases or not, as it was previously believed. The topic is much complex and there are broad discussions in the literature pointing out the controversies [2, 16, 18, 29].

It should be noted that both definitions are only indicative. For example, alloys with a small deviation in composition from the above definitions could be considered as HEAs. It is generally accepted that it is not necessary to strictly follow the definitions of HEAs due to wider composition restrictions to the evolution of novel alloys [30].

### **2.3 Four „core effects”**

The four „core effects” were believed to govern the HEAs behavior. This fact has been shown to be controversial, however, some of them may play an important role on the properties of this material, so they will be explained in the following sections. There are: the high entropy effect, the lattice distortion effect, sluggish diffusion, and the „cocktail effect”. Three of them are described as hypotheses and, the last one, known as the „cocktail effect” is a claim regarding HEAs, which was never proven. These hypotheses were initially evaluated according to the information available in the very earliest publications. In the following subchapters, these hypotheses are compared with the published data from the last 12 years [30, 31].

#### ***The high entropy effect***

The entropy for HEA mainly refers to configurational entropy in the literature [2]. For equimolar quinary random solid solutions and stoichiometric intermetallic compounds, their

value of configuration entropy was believed to be equal to  $1.61R$  ( $R = 8.31 \text{ J/K mol}$ ). According to Gibbs free energy difference:

$$\Delta G_{\text{mix}} = \Delta H_{\text{mix}} - T\Delta S_{\text{mix}} \quad (7)$$

, where  $\Delta G_{\text{mix}}$  [ $\text{J}\cdot\text{mol}^{-1}$ ] is Gibbs energy,  $\Delta H_{\text{mix}}$  [J] is enthalpy,  $T$  [K] is temperature and  $\Delta S_{\text{mix}}$  [ $\text{J}\cdot\text{K}^{-1}$ ] is the entropy of the system. In theory, the phases with higher entropy in alloys acquire lower Gibbs free energy. It follows that the high mixing entropy in HEAs was believed to support the formation of random solid-solution phases, rather than intermetallic phases. However, the high effect can not guarantee the formation of a simple solid solution phase in multicomponent alloys. In this case, we should take into account other important factors, such as other contributions of entropy, enthalpy mixing  $\Delta H_{\text{mix}}$ , size difference ( $\delta_r$ ), and some authors presented the concept of VEC [32, 33].

The mixing enthalpy  $\Delta H_{\text{mix}}$  in some cases of HEAs can have quite negative values and thus the formation of intermetallic compounds cannot be completely avoided. Accordingly, we can determine that the mixing enthalpy is another important characteristic parameter affecting the phase selection in HEAs. The mixing enthalpy in a random solid solution is defined as:

$$\Delta H_{\text{mix}} = \left( \sum_{i=1, j \neq i}^n \alpha_{ij} c_i c_j \right) \quad (8)$$

, where  $\alpha_{ij} = 4\Delta H_{\text{AB}}^{\text{mix}}$ , and  $4\Delta H_{\text{AB}}^{\text{mix}}$  is the mixing enthalpy for the binary AB alloy and  $c_i$  ( $c_j$ ) is the molar concentration of the  $i$ th ( $j$ th) atom.

The geometric factor and the atomic radius of the alloying elements in terms of deformation energy may also significantly affect the stability of the solid solution and the phase stability. According to Hume-Rothery rules [34], the atomic size difference between solvent and solute should not pass 15 % in binary solid solutions. In HEAs no specific solvent and solute elements are defines. Thus, some authors is a dispersion of atomic sizes to describe the stability of a solid solution. The parameter  $\delta_r$ , related to the atomic size difference is defined [35-37] as:

$$\delta_r = \sqrt{\sum_i^n c_i \left(1 - r_i/\bar{r}\right)^2}, \quad \bar{r} = \sum_i^n c_i r_i \quad (9)$$

, where  $r_i$  is the atomic radius of the  $i$ th atom.

In HEAs, many crystallographic systems can be presented, but the most reported ones are BCC and FCC, solid solutions structures. In conventional alloys with a base element, the choice of the structure is commonly considered from the effects of the supplementary elements (solute atoms) on the structure of the major element (solvent atom). There are several major elements in HEAs for which we can no longer directly apply traditional considerations about structure selection. Some studies have shown that valence electron concentration (VEC) is a dominant factor that controls the structure of FCC and BCC solid solutions in some groups of

HEAs, provided that only solid solutions would form and no intermetallic compounds are formed [36, 38]. The VEC in HEAs is defined as:

$$\text{VEC} = \sum_i^n c_i(\text{VEC})_i \quad (10)$$

, where  $(\text{VEC})_i$  is the valence electron numbers for the  $i$ th atom.

Based on limited experiments on HEAs obtained so far, both the mixing enthalpy and atomic size difference are significantly involved in the regulation of phase stability in HEAs. Although the parameters of  $\Delta H_{\text{mix}}$  and  $\delta_r$  are based on observation or experience and the physical significance of VEC is not well understood, especially for certain groups of HEAs, these experimental parameters provide useful conduction for phase selection in some HEAs [36].

According to Gibbs free energy (equation 7), the effect of high entropy on the stability of random phases of a solid solution decreases with decreasing temperature. It follows that random phases of solid solution can be converted into intermetallic phases if the HEAs were annealed at a relatively low temperature [33, 39, 40]. For example, refractory HEA HfNbTaTiZr has only one BCC phase after homogenization annealing. However, the HCP phase is improved with Hf and Ta (approximately 25 at. % each) and was observed in the BCC matrix after annealing at 600 or 800 °C [40]. It should be pointed out that in some cases intermetallic phase may sometimes improve the properties of HEAs, which follows that HEA research should not be limited to simple solid-solution phases [33].

### ***The sluggish diffusion effect***

Diffusion may be expected to be sluggish in HEAs [31]. This statement is based on secondary observations, which include the formation of nanocrystals and amorphous phases upon solidification, and on qualitative analysis of microstructural stability upon cooling. To further support this stand, general observations relating to difficulty in substitutional diffusion and high activation energies are called into use [2, 33].

The occurrence of nanocrystals in as-cast  $\text{Al}_x\text{CoCrCuFeNi}$  [41] and retention of nanocrystals in  $\text{AlCrMoSiTi}$  after annealing [30] were clarified to be a sign of slow diffusion. Furnace cooling of  $\text{Al}_{0.5}\text{CoCrCuFeNi}$  keep away from formation of low-temperature phases, and  $\text{AlMoNbSiTaTiVZr}$  is a better diffusion blockade than TaN/ TiN or Ru/TaN [42]. Both of these results have been used to explain the sluggish diffusion hypothesis. However, alternate analyses provide us equally satisfying explanations for all of these examinations. As a starting point for comparison are used conventional alloys, nanometer-sized precipitates remain in superalloys for tens or hundreds of hours at temperatures that come close to 85 % of the absolute melting temperature ( $T_m$ ). While the above indirect observations are consistent with slow kinetics, they do not indicate that diffusion is slower for HEAs compared to conventional alloys [43]. Also, the compositional complexity of HEAs makes it difficult to measure diffusion [29].

From the latest data, we can conclude that diffusion coefficients in  $\text{CoCrFeMn}_{0.5}\text{Ni}$  are not significantly different from diffusion in elements and conventional alloys. This conclusion is

based on a comparison of the available results of measured diffusion coefficients for FCC metals and alloys at  $T_m$ . It further supports the fact that all data measured in Ref. [42] all belong to a single order of magnitude, both before and after normalization by  $T_m$ .

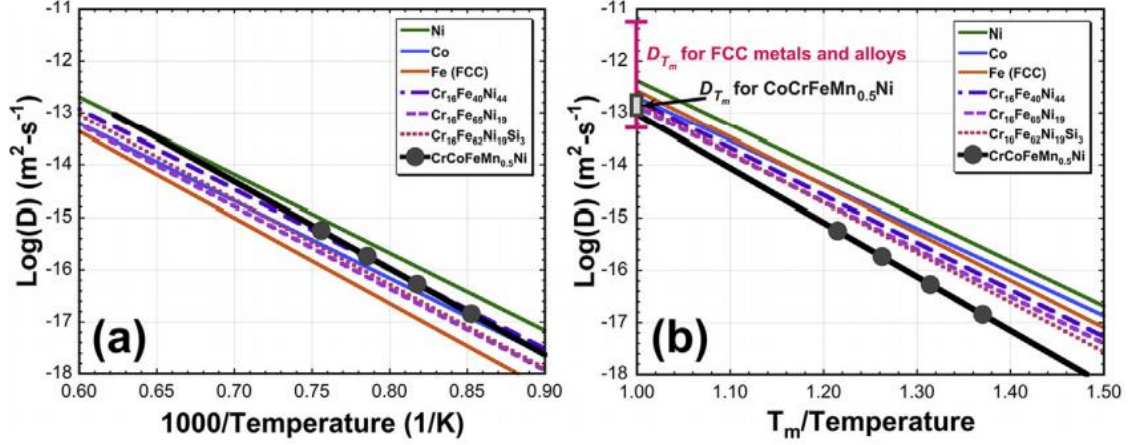


**Fig. 2** Diffusion coefficients of Ni ( $D_{Ni}$ ) in FCC elements, stainless steel, and CoCrFeMn<sub>0.5</sub>Ni as a function of (a) inverse absolute temperature, and (b) inverse absolute temperature normalized by the melting or solidus temperature of the host alloy,  $T_m$  [29].

In conclusion, data that support the sluggish diffusion hypothesis are obtainable only for certain high entropy alloys, and a larger dataset is needed to better investigate the hypothesis that unusually slow diffusion can be possible in HEAs as a class of materials [44].

### *The lattice-distortion effect*

Severe lattice distortion is based on the different sizes of atoms that form crystal lattices of complex, concentrated phases, as shown in Fig. 3. The displacement at each location of the lattice depends on the atom occupying that location, and on the types of atoms in the local environment. It is claimed that these distortions tend to be more severe than in conventional alloys [14, 31].

Lattice distortion affects the hardening of the solid solution and contributes to excessive configurational entropy. It is also involved in the difficulty of distinguishing between ordered and disordered phases using the standard X-ray diffraction technique. Crystal lattices in the HEAs are almost certainly affected by distortion, but there is no systematic evidence to directly confirm this. The  $\delta_r$  parameter is commonly used to determine the variability in atom sizes, but in this case, the distortion in the structure can be less. For example, distortion is lower in structures where the 1st shell surrounding a smaller atom which is mainly populated by larger atoms, and where larger atoms are surrounded by smaller atoms. An approach to measure and model lattice distortion is necessary [29].

At present, there seems to be only one type of experimental method that can be used to measure lattice distortions [45]. Lattice fringes are detected on inverse fast-Fourier transform (FFT) images, which are taken from high-resolution transmission electron microscopy photographs.

Future work is focused on quantification of the magnitude of lattice distortion and isolating its effect [29].

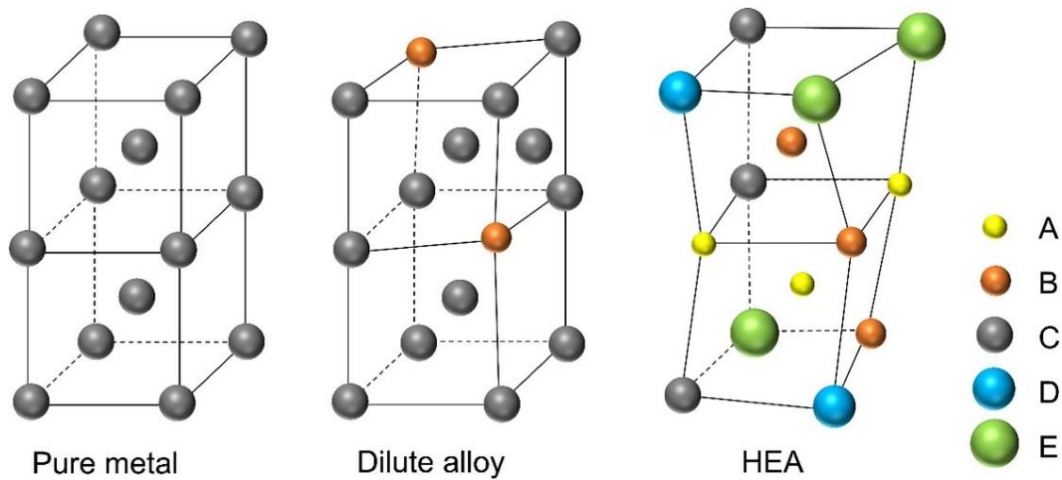


**Fig. 3** Schematics of lattice distortion in body-centered cubic pure metals, conventional dilute alloys and high entropy alloys. A–E represents different element species [46].

### *The ‘cocktail effect’*

Unlike the other ‘core effects’, the ‘cocktail effect’ is not a hypothesis and no evidence is required. The phrase was first used by prof. S. Ranganathan and his initial aim was simple, ‘a pleasant, enjoyable mixture’. Although, it later came out to represent a synergistic mixture where the final result is unpredictable and bigger than the sum of the parts [47]. This phrase was introduced to express three different alloy classes: bulk metallic glasses, super-elastic and super-plastic metals, and HEAs. Each of these alloy classes covers complex, concentrated alloy compositions. The ‘cocktail effect’ is primarily focused on the outstanding properties of fully amorphous bulk metallic glasses and the structural and functional properties of super-plastic metals, such as ultra-high strength with good fracture, weaker resistance, and ductility. In each of these cases, resulting properties depend on material composition, microstructure, electronic structure, and other functions in complicated and delicate ways. The ‘cocktail effect’ reminds us to stay open to non-linear, unpredicted results that can come from unusual combinations of elements and microstructures in the enormous composition space of HEAs [29].

## **2.4 Preparation and Processing**

According to the existing researches and application experience, the traditional preparation method of HEAs is basically the same as the preparation methods of conventional alloys. However, the existence of the difference is undoubted. HEAs have various forms such as bulk, films, belt, powders, and fibers. Based on this, HEAs are usually manufactured as four types in line with their dimension, as demonstrated in Fig. 4: bulk HEAs (three-dimensional HEAs), high entropy films and coatings (two-dimensional HEAs), HEA fibers (one-dimensional HEAs), and HEA powders (zero-dimensional HEAs) [48, 49].

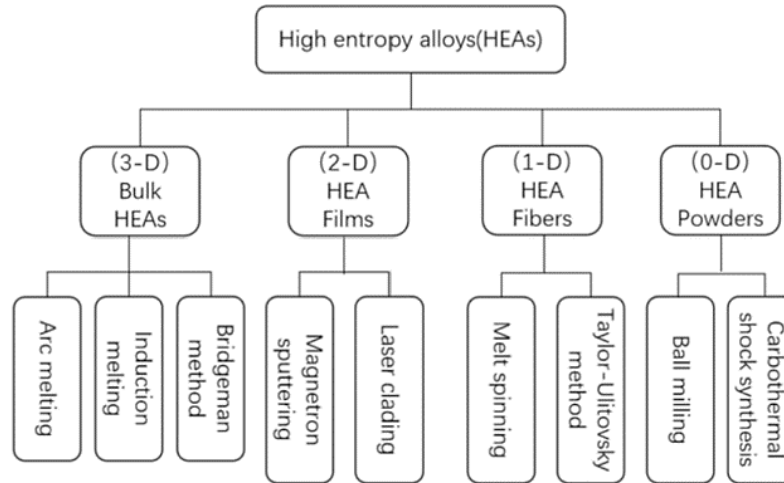


**Fig. 4** Classification of HEAs according to preparation size [49].

Traditional preparation methods of three-dimensional HEAs mostly include vacuum arc melting, vacuum induction melting, mechanical alloying and subsequent sintering, and so on. Certain preparation methods lead to directional solidification, which can be used to obtain a certain orientation of the crystals [50]. It should be noted, that the experimental high entropy alloy  $\text{Al}_{0.2}\text{Co}_{1.5}\text{CrFeNi}_{1.5}\text{Ti}$ , applied in this study, was produced by vacuum induction melting. Therefore, we will deal with this technique in more detail in the following section: preparation by vacuum induction melting.

According to the newest publications, there are also several new methods for preparing bulk HEAs, such as high-gravity combustion synthesis and additive manufacturing. Chen et al. [51] investigated the implementation of additive manufacturing methods in the production of HEAs. Compared to casting counterparts, it has been found that HEAs prepared by additive manufacturing may have a superior yield strength and ductility due to the fine microstructure formed during the rapid solidification in the fabrication process. As a result, this is an effective method for improving their comprehensive properties. Various processing methods are closely connected to the performance.

Annealing, as an efficient method, has been introduced to improve the microstructure and properties of alloys, where the different annealing temperatures and time are closely related to comprehensive properties. Zhuang et al. [52] examined the effect of annealing temperature on the microstructure, and mechanical properties and phase constituents of  $\text{Al}_{0.5}\text{CoCrFeMo}_x\text{Ni}$  ( $x = 0, 0.1, 0.2, 0.3, 0.4, \text{ and } 0.5$ ) HEAs at the specified annealing time (10 h). They found that the alloys annealed at  $80\text{ }^\circ\text{C}$  exhibited higher hardness and yield strength, due to the relatively fine precipitates and resulting microstructures. Sathiyamoorthi et al. [53] insert a high-pressure torsion-treated CoCrNi alloy with a grain size of  $\sim 50\text{ nm}$  into different annealing conditions and investigated the optimal processing technology. The sample annealed at  $700\text{ }^\circ\text{C}$  for 15 min showed an impressive combination of the tensile strength ( $\sim 1090\text{ MPa}$ ) and strain to failure ( $\sim 41\%$ ).

The pressure is considered to be another essential and powerful parameter, introduced to the experimental study of HEAs. Many interesting reversible/irreversible phase transitions that were not previously expected or otherwise invisible were observed under high pressure. Zhang et al. [54] reviewed recent outcomes in various HEAs achieved by using in situ static high-pressure synchrotron radiation X-ray methods and come up with new prospects for future investigation.

Welding is an important area with a high potential effect on future research and technological developments in the field of HEAs. The selection of possible welding processes with optimized parameters is required to improve applications of HEAs. Guo et al. [55] examined recent works on welding of HEAs in detail with a focus on the research of HEA systems in the application of different welding methods.

### ***Preparation by vacuum induction melting***

Among the reported traditional preparation methods (Fig. 4) most bulk HEAs are produced by liquid state route, including vacuum induction melting. The metal is under vacuum exposed to deep degassing, resulting in a perfectly deoxidized metal along with a homogenized bath due to the bath mixing. As a result, alloy prepared by this technique contains a very low content of non-metallic inclusions. Additionally, with the help of vacuum induction furnaces, it is possible to melt alloys with any chemical composition within the temperature limitation range of the machine [56].

However, there are some attention problems using this type of technology for preparing HEAs, as emphasized in the following: the solidification process cannot be well controlled due to the nature of rapid solidification, leading to different microstructure characteristic from the surface to the center of alloy samples, e.g., inhomogeneous separation of the as-cast dendrites in morphology and size, line up from fine grains to columnar dendrites and thus an unmanageable macroscopic property. Also, a series of unavoidable as-cast defects, along with elemental segregation, suppression of equilibrium phases, microscopic and macroscopic residual stresses, cracks, and porosities, may have a negative effect on the mechanical properties of HEAs. Measures should be taken into account to reduce or eliminate these defects in the HEAs [57].

## **2.5 Microstructures of High Entropy Alloys**

HEAs produced by the casting route show typical cast microstructure consisting of dendritic (DR) and interdendritic (ID) regions. DR region is often found to exhibit microstructural features such as precipitates, nanostructured phases, and modulated structure arising from spinodal decomposition (SD), whereas the ID region was shown to exhibit a two-phase eutectic structure [1].

Singh et al. [58] studied the microstructure of the AlCoCrCuFeNi alloy. The phase formation sequence is shown, in detail in Fig. 5.

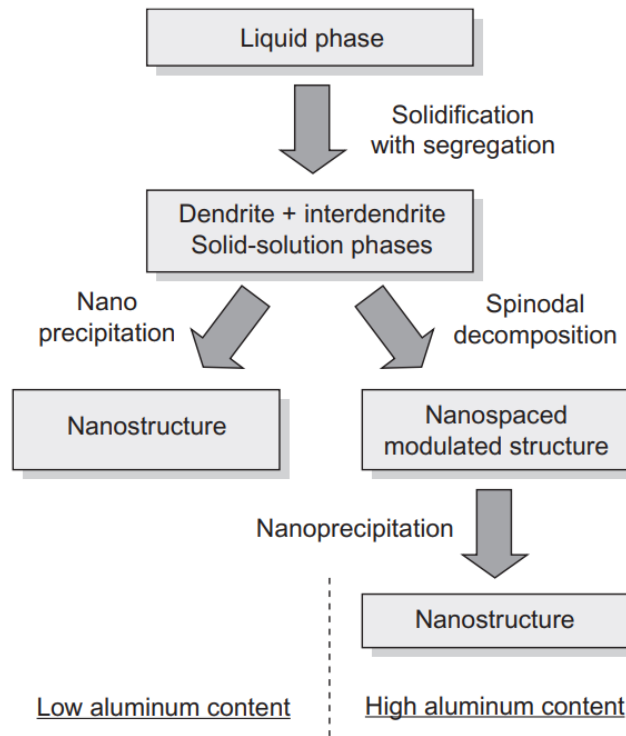


**Fig. 5** Depiction of phase formation sequence during cooling of  $\text{Al}_x\text{CoCrCuFeNi}$  alloy system with different aluminum contents [14].

Tung et al. [59] discussed the microstructural properties of various HEAs, which contain different elements in non-equiatomic proportion. In alloys with lower copper content ID regions appeared, visible from the segregation tendency of the element. SD leading to modulated structures, which can be observed in alloys containing BCC phase (DR regions), while ID regions have heterogeneous FCC and BCC structures. From these results, it can be deduced that although the configurational entropy for various alloys is the same, their microstructure differs are obvious in terms of phase fractions and compositions, further underlined by the fact that other thermodynamic factors also play a role in phase evolution in non-equiatomic HEAs.

They observed the microstructure of DR (Fig. 6) in as-cast alloys (Label. A), resulting in a claim that the DR region consists of many secondary phases such as plate-like precipitates (Label. B), rhombohedral and spherical precipitates (Label. C), and weak superlattice reflections of  $\text{L1}_2$  phase. The DR region has also been shown to contain NiAl, CrFe, and Cu-rich plates as studied by 3D atom probe. On the other hand, splat-quenched  $\text{AlCoCrCuFeNi}$  alloy, shown a polycrystalline microstructure with clear grains and grain boundaries [59].

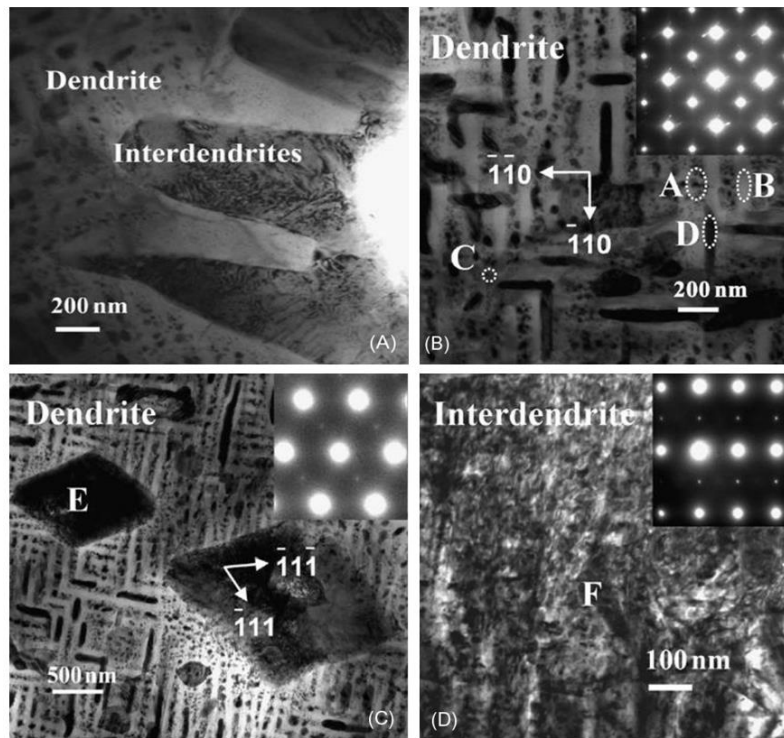


**Fig. 6** Bright-field TEM images showing (A) DR and ID regions; (B) DR showing plate-like precipitates and presence of ordered B2 structure; (C) presence of rhombohedral precipitates in DR and weak reflections of L<sub>12</sub> phase; and (D) microstructure of ID region and weak superlattice reflections of L<sub>12</sub> phase for as-cast AlCoCrCuFeNi alloy [14].

In contrast to the above observation on cast alloys, atom probe studies on mechanically alloyed (MA) CoCrFeNi HEAs suggest an even distribution of alloying elements in the as-milled condition. However, segregation of specific elements after hot consolidation has been observed in some alloys prepared by MA. Elemental atom probe mapping tomography in AlCoCrCuNiZn HEA prepared by MA followed by hot compaction at 600 °C showed Cu segregation at grain boundaries. After consolidation, retention of nanocrystalline grains was also examined with a size of about 10nm [14].

Over the processing methods, the resulting microstructure of HEAs also depends on the alloying element. As a consequence the phase equilibrium among kinetics changes in the solidification stage. For example, the addition Ti to AlCoCuFeNi, resulting in changes of morphology from DR to eutectic cell type (Wang et al., [60]) while the V addition exhibits DR region with ellipsoidal particles instead of modulated plate-like structure. These phenomena are more revealed in the general properties section.

Mechanically alloyed powders of non-equiatomic HEAs compared to equiatomic HEAs show similar microstructure characteristics features, such as hard agglomerates, smooth fine particles, and uniform morphology. Chen et al. [61] prepared AlCoCrCu<sub>0.5</sub>FeMoNiTi alloy by MA. According to the mechanisms of MA, the 2 h-milled powders exhibited lamellar structures which transform into the uniform amorphous microstructure after 36 h of milling. In a similar study by Sriharitha et al. [62] alloy Al<sub>5</sub>CoCrCuFeNi prepared by MA, the microstructure exhibited an average particle size of about 0.5 microns with a crystallite size less than 50 nm.

Besides, the development of advanced techniques such as high-resolution transmission electron microscopy, atom probe tomography, electron backscattered diffraction (EBSD), etc. shown to be very useful in detecting the fine microstructural details of HEAs [14]. Thus we can conclude that very different microstructural features can be obtained except for single phase solid solutions. These can bring improved properties to the alloys.

### 2.6 General Properties

Mechanical behavior is one of the most extensively studied researches in the field of HEAs. The main research is focused on three types of alloys: 1, 3D transitional-group-element HEAs; 2, 3D transitional-group-element HEAs with Al or Ti added; 3, refractory high entropy alloys with excellent high-temperature properties. Furthermore, other trace alloying elements, such as Mo, Nb, Zr, etc., were put into use in order to study their effect on the microstructures and properties of the alloys.[50].

HEAs metals based on 3D transition such as CrCoNi and CrMnFeCoNi alloys, exhibit prominent mechanical properties like strength and fracture resistance, as emphasized in Asby’s map of construction materials (Fig. 7). Fig. 8 represents the influence of temperature on tensile properties and fracture toughness of the CoCrFeMnNi. The alloys exhibit a very good combination of ductility and fracture, which increases with decreasing temperature. This combination of properties makes Cantor’s alloy unique because most materials become more brittle as the temperature is decreased. In this case, the values of crack-initiation toughness exceed ( $K_{IC}$ ) more than  $200 \text{ MPa}\cdot\text{m}^{-1/2}$  independent of the temperature [18].

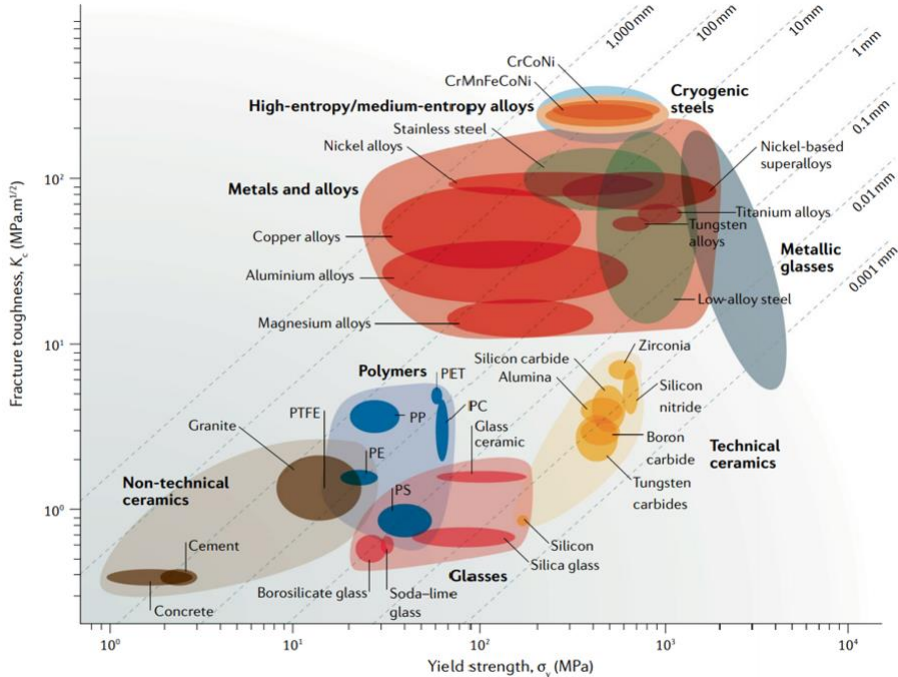
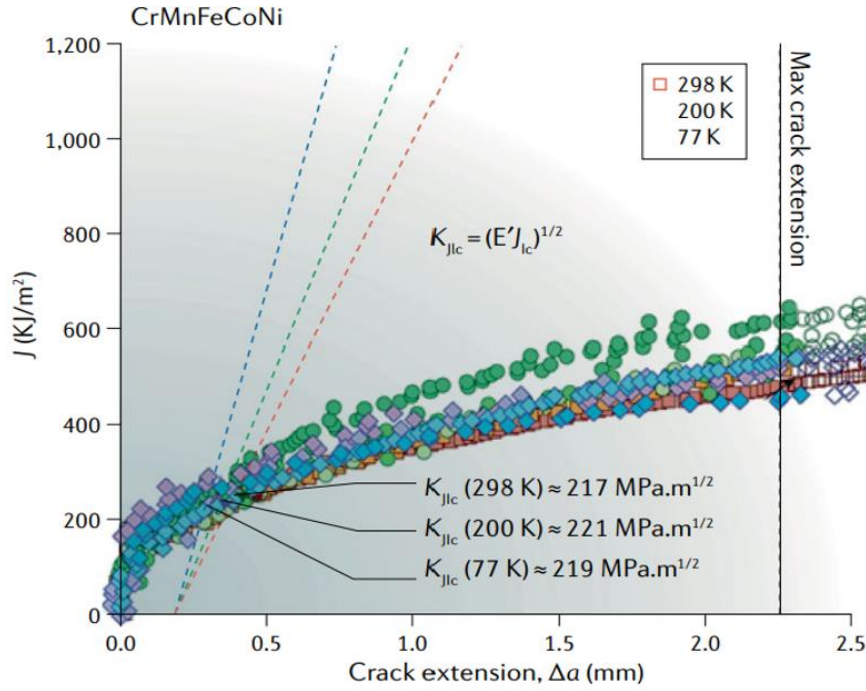


Fig. 7 Ashby plot of strength versus fracture toughness of CrCoNi-based, medium-entropy, and high entropy alloys [18].



**Fig. 8** Crack resistance curves of the Cantor alloy CrMnFeCoNi [18].

Additional elements such as Nb significantly support the reduction of nano-phases and thus increase the strength of the alloy [63, 64]. The addition of Mo to the CoCrFeNi alloys effectively helps to increase the corrosion resistance [65]. The effect of adding Zr to the CoCrFeNiMn alloy was investigated by Zhang et al. [66]. The alloys were prepared from ZrH<sub>2</sub> powders using a mechanical alloying technique. The results indicate, that multiphase microstructures were formed in the alloys, which can be attributed to the large lattice strain and negative enthalpy of mixing, caused by the addition of Zr. Sun et al. [67] also used a mechanical alloying technique to prepare a CoCrNiCuZn alloy. The addition of Pd promoted local and long-range lattice distortions in CoCrFeNi alloy, which affects the phase stability and phase transformation. The addition of elements such as Al and Ti in 3D transition CoCrFeNi HEAs exhibits a strong impact on microstructure and phase composition. Alloying elements such as Al and Ti in 3D transitional CoCrFeNi HEAs show a strong influence on microstructure and phase composition, as well as the ability to reduce the density.

Due to its excellent mechanical properties, high entropy films processed by magnetron sputtering technology attracted attention with their exciting potential for the production of small-structure devices and precision instruments with sizes ranging from nanometers to micrometers. Zhang et al. [68] fabricated (Al<sub>0.5</sub>CrFeNiTi<sub>0.25</sub>) high entropy films. It has been exhibited that the phase structure varies from the amorphous to the FCC structure with increasing nitrogen content, which is closely related to the atomic size difference in the alloy system.

It can be found that nano-precipitation phases extensively appear in HEAs, which play an essential role in improving their mechanical properties such as strength and plasticity. Wang et al. [69] described the precipitation behavior and precipitation strengthening in HEA detailedly, including the morphological development of second-phase particles and the

mechanisms of precipitation strengthening. They argue that the challenge for the future is to design a stable and coherent microstructure in different matrices of solid solutions.

Besides mechanical properties at room temperature, HEAs tend to exhibit excellent properties at higher temperatures due to the high-entropy stabilization effect. The Hf-Nb-Ta-Ti-Zr refractory HEA shows remarkable properties at high-temperature as well as at room temperature. Zýka et al. [70] presented a study of the tensile mechanical properties at room temperature of selected three- and four-element medium entropic alloys derived from the Hf-Nb-Ta-Ti-Zr system and found that it is a five-element HEA alloy that shows the best combination of strength and elongation. Tseng et al. [71] focused on revealing the effects of Mo, Nb, Ta, and Ti on the mechanical properties of equiatomic alloys Hf-Mo-Nb-Ta-Ti-Zr.

Wear resistance and tribological behavior also play an important role in materials development. Wear properties have been investigated since the early stages of HEA development, although the data set is still limited. For example, Chuang et al. [72] reported outstanding adhesion to wear resistance of  $\text{Al}_{0.2}\text{Co}_{1.5}\text{CrFeNi}_{1.5}\text{Ti}_y$  HEA, with a hardness of 717 HV and a resistance 3.6 times that of SUJ2 with similar hardness. Furthermore, the HEA exhibits twice as high wear resistance as high-speed tool steel SKH51 with a hardness of 870 HV. They showed that this excellent performance is due to its remarkable oxidation resistance and hot hardness compared to comparable steels, as the contact temperature at the pin-disk interface can reach values of up to 80 °C [14].

In addition to mechanical properties, research is also focused on the physical and chemical properties of HEAs such as magnetic properties, radiation resistance, electrical properties, and corrosion resistance [50].

### 3 Aim of the work

The  $\text{Al}_{0.2}\text{Co}_{1.5}\text{CrFeNi}_{1.5}\text{Ti}$  high entropy alloy and its variants have stood out as potential real alternatives for applications in which high wear resistance is required, due to their excellent wear resistance combined with high strength. Despite the very interesting properties, these alloys possess low ductility due to their complex microstructure.

In this work, the mechanical characteristics and microstructural evolution of  $\text{Al}_{0.2}\text{Co}_{1.5}\text{CrFeNi}_{1.5}\text{Ti}$  HEA produced by vacuum induction melting, followed by casting and subsequent annealing at various temperatures (750 °C and 1000 °C), were studied. The heat treatment experiments were performed with the intention of improving the mechanical properties of the HEA, such as better ductility. This could be done by reducing the content of intermetallic phases present in the alloy. A calculation of the pseudo binary phase diagram (CALPHAD) was performed to evaluate the possible phases present on the alloy. Additionally, the experimental part was done by X-ray diffraction (XRD), scanning electron microscopy (SEM), and energy dispersive spectroscopy (EDS) analyses of the HEA in all states. These were performed to reveal the phase, microstructures, chemical composition, and crystallographic properties. The mechanical properties evaluation related to different microstructures of the alloy were characterized using micro-Vickers hardness and nanoindentation testing by analyzing the hardness of the produced material.

## 4 Experimental material and methods

### 4.1 Experimental material preparation

The  $\text{Al}_{0.2}\text{Co}_{1.5}\text{CrFeNi}_{1.5}\text{Ti}$  HEA was prepared by vacuum induction melting from elemental components with purity higher than 99,5 wt. %. In order to ensure the surface cleanliness of the melting batch, dry blasting was performed. The ceramic crucible (Fig. 9b) was made of pressed zircon material ZC93i and formed into an inductor of an induction medium frequency vacuum furnace. A permanent mold was prepared for melting, where the inner part was covered with a spray of yttrium oxide. This was followed by controlled heating on an electric resistance furnace according to the manufacturer's recommendations with a delay of at least 500 °C and a gradual decrease to a final temperature suitable for casting, approx. 200 °C, which has been formed into a casting module. Therefore, the smelting process was carried out in an induction medium frequency vacuum furnace (ISVP), shown in Fig. 9a, on a basic charge of pure iron, with gradual alloying in a vacuum according to the affinity series of individual elements of the batch for oxygen. After achieving optimal melting of the total batch at a pressure of 4 Pa in the ISVP caisson, the alloy was cast into a casting module located in an argon atmosphere. The melt was left in a closed caisson to minimize the cooling rate of the ingot. In compliance with the above technological and metallurgical procedures, the surface of the ingot was without any defects and the crystallization zones in the ingot were satisfactory.



**Fig. 9** Heraeus vacuum induction equipment in VUT FSI for melting, processing, and casting in vacuum or an inert atmosphere (max. Approx 20k) (a) vacuum induction furnace IS2/ I HERAEUS; (b) zirconia ZC93i crucible for metal handling and melting.

## 4.2 Characterization methods

The cut-off machine Brillant 220 (Metalco Testing s.r.o) was used to cut the base material into 3 samples with approximate dimensions of 20 mm length, 6 mm width, and 6 mm depth. Afterward, the preparation of bulk samples for microstructural investigations was mostly carried out by hot mounting using black epoxy resin DuroFast with mineral filler. Once the samples were hot mounted in resin, they were mechanically ground with SiC abrasive papers of different particle sizes #220-2400 grit. Subsequently, the samples were polished using diamond paste with a particle size of 3  $\mu\text{m}$  and 1  $\mu\text{m}$ . The last step of sample preparation was mechanical-chemical polishing with OP-S F. The following metallographic technique was applied to the first sample immediately, and for the other two samples after heat treatment experiments.

### *X-ray diffraction (XRD)*

X-ray diffraction analysis of the materials phase composition was done using Philips X'Pert Pro diffractometer operated at 40 kV voltage with 30 mA current. A continuous scanning was done with  $2\theta$  between  $30^\circ$  and  $100^\circ$  using a speed of  $0.02^\circ \cdot \text{min}^{-1}$  and a step size of  $0.0167^\circ$ . The radiation used was Cu-K $\alpha$ .

### *Scanning electron microscopy (SEM)*

Scanning electron microscopy (SEM) characterization of the bulk materials in as-cast state and after heat treatments was performed using ZEISS Ultra Plus FED microscope in secondary (SE) and backscattered electron (BSE) modes. Energy-dispersive X-ray microanalysis studies (EDS) were performed to evaluate the chemical composition of the material.

### *Calculation of Phase Diagrams (CALPHAD)*

Calculation of phase diagram (CALPHAD) was performed using ThermoCalc software version 2020b (TCHEA4 database version 4.1).

### *Micro Vickers hardness*

Vickers hardness measurements were carried out according to ISO 6507-1 standard using a Qness Q10A microhardness tester with an applied load of 0.2 kg. The reported values for the materials in a cast state and after heat treatment experiments are on average of at least 15 measurements and the error is the standard deviation.

### *Nanoindentation hardness*

Nanoindentation experiments were performed in order to determine the elastic modulus of the as-cast material in line with the Oliver-Pharr method [73]. CSM Instruments nanoindenter tester with a pyramidal Berkovich diamond indenter was used at an acquisition rate of 10 Hz, the maximum force of 100 mN, with load/unload rates of  $200 \text{ mN} \cdot \text{min}^{-1}$  and hold period of 10 s. For each sample the averages of at least 25 indents are presented, where the error is the standard deviation of the measurements.

### ***Heat treatment experiments***

Heat treatment effect on experimental material  $\text{Al}_{0.2}\text{Co}_{1.5}\text{CrFeNi}_{1.5}\text{Ti}$  HEA presented in this study was performed in an annealing furnace ELSKLO type MF5, in order to investigate the influence of the temperature and time of annealing on the evolution of the microstructure. The as-cast samples were heat-treated in a furnace using air atmosphere at 1000 °C for 5h, labeled as C01, and at 1000 °C for 5h with subsequent 750 °C for an additional 5h, labeled as C02.

## 5 Results and discussion

### 5.1 Calculation of phase diagrams - CALPHAD

The  $Al_{0.2}Co_{1.5}CrFeNi_{1.5}Ti$  high entropy alloy pseudo binary phase diagram was calculated with the help of ThermoCalc [74] software using the TCHEA4 database [75, 76], where the theoretical composition of the HEA is shown in Table 1 below. A calculated pseudo binary phase diagram of the  $Al_xCo_{1.5}CrFeNi_{1.5}Ti$  HEA for different mole percent Al is shown in Fig. 10. The alloy proposed in this study possesses 3.2 at. % Al, highlighted by a red arrow. Fig. 11 represents a scheme of property diagram as mole fraction versus temperature. It can be seen that the phase constitution in the high entropy alloys changes continuously with the alloy compositions and the temperatures. It should be noted that the phase diagram was calculated previously by Moravcikova-Gouvea et al. [77], however, the present phase diagram shown in this study is a more updated version with the new TCHEA4 database, instead of TCHEA3.

**Table 1** Theoretical composition of the as-cast  $Al_{0.2}Co_{1.5}CrFeNi_{1.5}Ti$  high entropy alloy.

Name of alloy	Composition of the alloy (mole fraction)					
	Al	Co	Cr	Fe	Ni	Ti
$Al_{0.2}Co_{1.5}CrFeNi_{1.5}Ti$	0.0323	0.2419	0.1613	0.1613	0.2419	0.1613

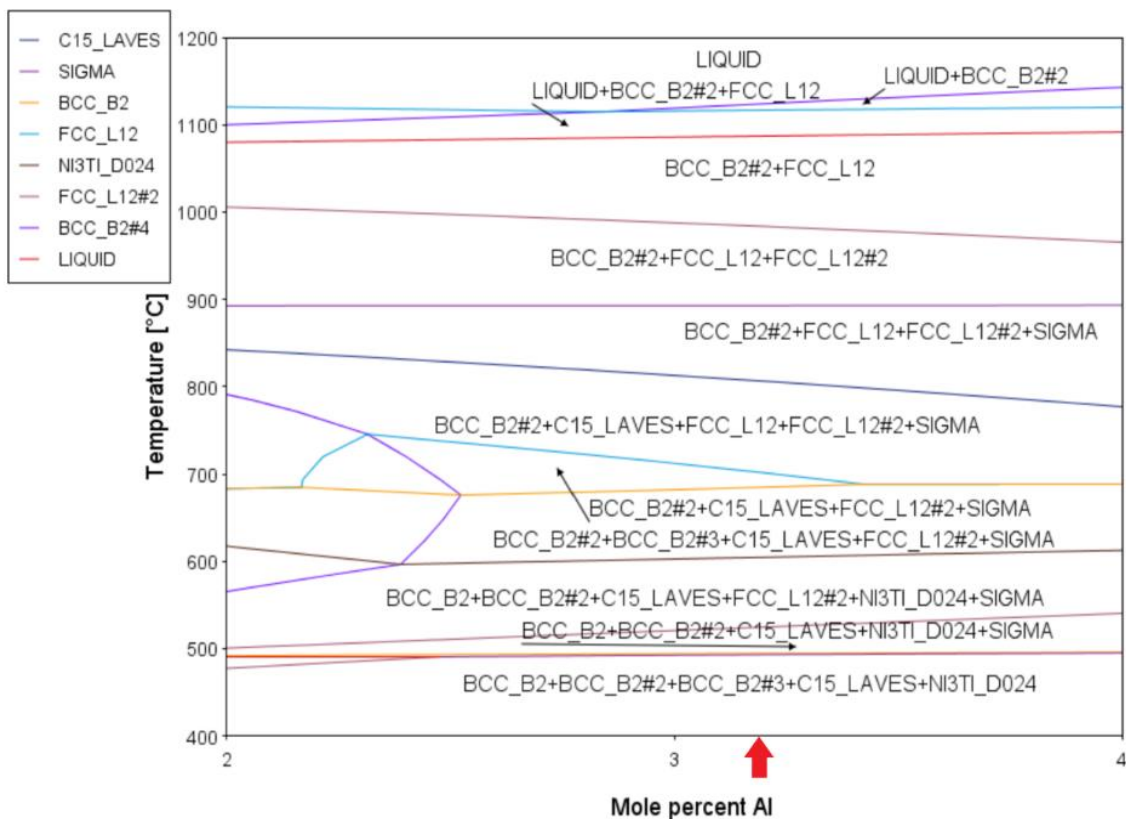


**Fig. 10** CALPHAD calculation of the phase diagram for  $Al_{0.2}Co_{1.5}CrFeNi_{1.5}Ti$  high entropy alloy:  $Al_xCo_{1.5}CrFeNi_{1.5}Ti$  calculated phase diagram, where x range from 2 mole percent up to 4.

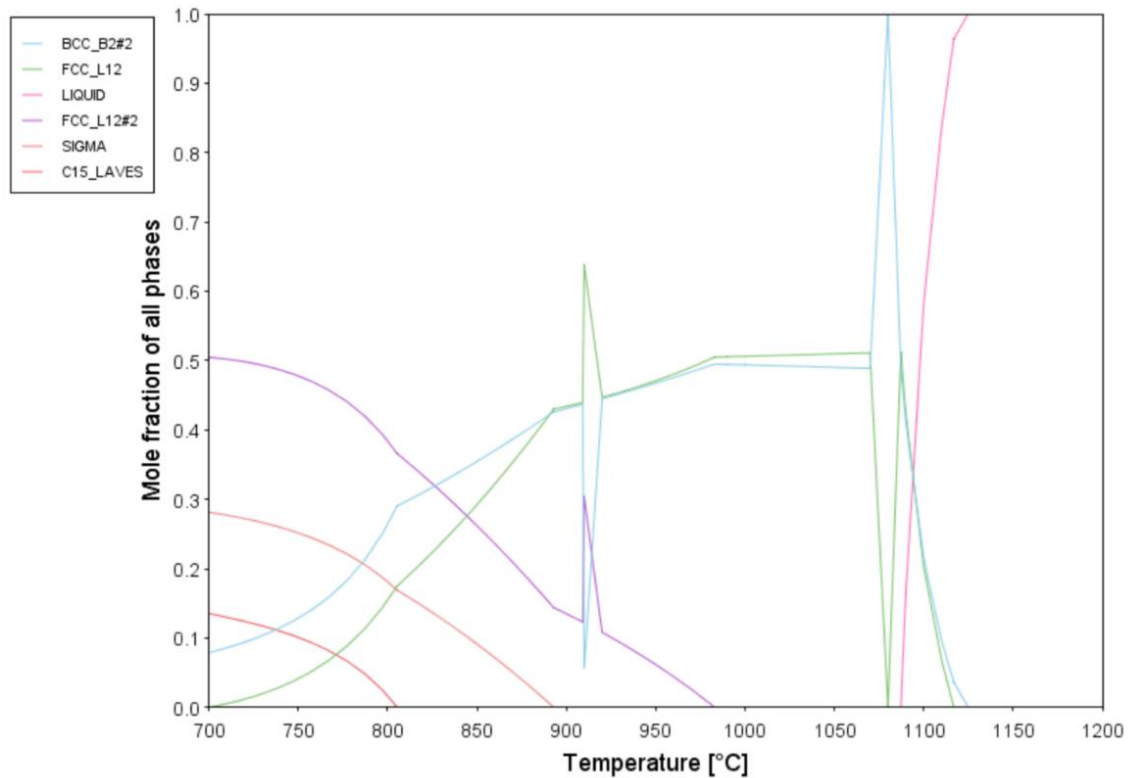


**Fig. 11** CALPHAD calculation of the property diagram for  $\text{Al}_{0.2}\text{Co}_{1.5}\text{CrFeNi}_{1.5}\text{Ti}$  high entropy alloy as mole fraction of all phases versus temperature.

During solidification, the simulation predicts the formation of BCC\_B2#2 structure as the first solid phase from liquid, while all the liquid phase is transformed into BCC\_B2#2 and FCC\_L12 structures at around 1120 °C. The first FCC\_L12#2 structure starts to precipitate out from BCC\_B2#2+FCC\_L12 structure at around 1080 °C, while the sigma phase begins to precipitate out around 880 °C. Since the sigma phase has a very brittle character, its content could be reduced by proper thermal treatments [67]. The annealing temperature should be higher than its lowest dissolving temperature 880 °C and therefore is set to be 750 °C. Meanwhile, the CALPHAD simulations show the subsequent formation of C15\_Laves with a gradual decrease in temperature below 810 °C.

## 5.2 XRD analysis

The XRD patterns of the as-cast and annealed  $\text{Al}_{0.2}\text{Co}_{1.5}\text{CrFeNi}_{1.5}\text{Ti}$  HEA are shown in Fig. 12, where the background changes are a result of the influence of amorphous parts. It should be noted, that the detected phases were pointed out in the C01 sample as a reference. However, all phases are found in all alloys, except for Hexagonal  $\text{D0}_{24}$  which was present only in C01 and C02. In this light, the C01 was chosen as the reference, as it contains all phases.

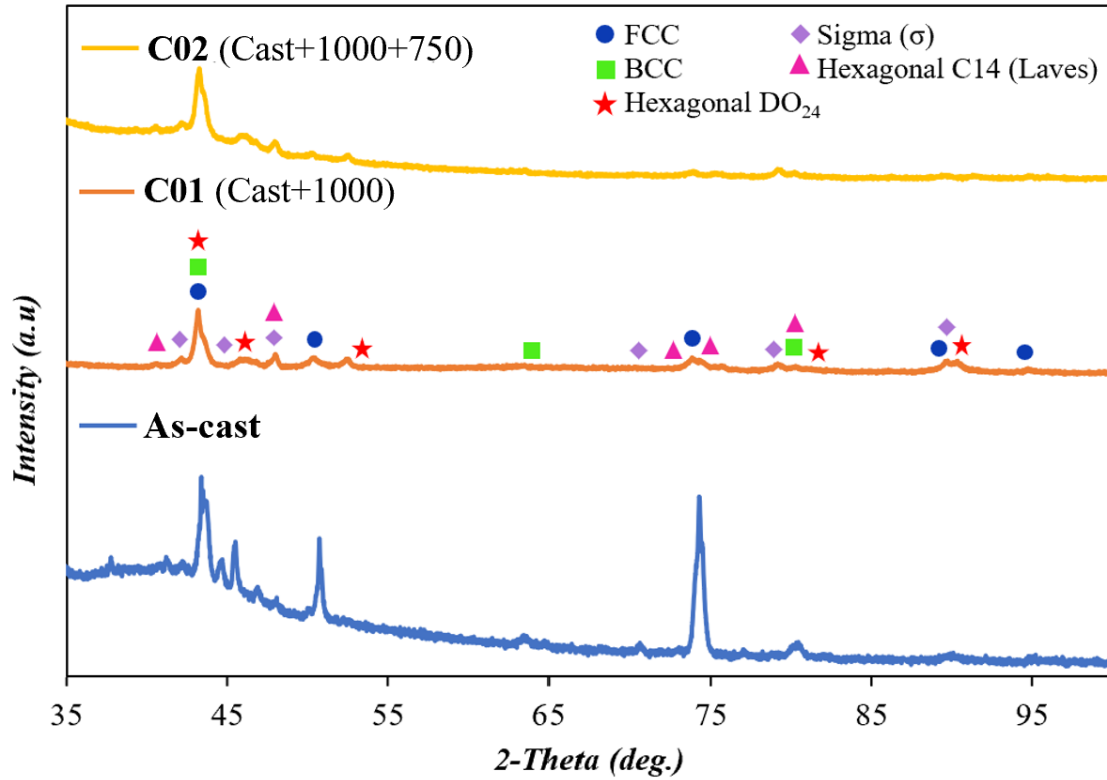


**Fig. 12** XRD patterns for the as-cast and annealed (C01 and C02)  $\text{Al}_{0.2}\text{Co}_{1.5}\text{CrFeNi}_{1.5}\text{Ti}$  high entropy alloys.

XRD analysis of the as-cast showed the presence of a major FCC phase, whereas the presence of the BCC phase was observed in the smallest amount. Table 2 shows the phases detected by the XRD method, including the wt. % and their respective crystal structures.

**Table 2** Phases present in the as-cast sample of  $\text{Al}_{0.2}\text{Co}_{1.5}\text{CrFeNi}_{1.5}\text{Ti}$  high entropy alloy.

<i>As-cast</i>	
<i>Crystal structure</i>	<i>Wt. %</i>
Ni (FCC)	47.8
Fe (BCC)	10.1
CrFe (Sigma)	11.5
Hexagonal C14- $\text{Fe}_2\text{Ti}$ (Laves)	30.6

XRD analysis of C01 alloy showed a decrease in the relative amount of Laves phase in comparison to the as-cast alloy, after heat treatment at 1000 °C for 5h. The phases found on this alloy are shown in Table 3. After heat treatment at 1000 °C for 5h, followed by 750 °C for an additional 5h, the C02 alloy exhibits a different microstructure, with phases shown in Table 4.

**Table 3** Phases present in the annealed sample of Al<sub>0.2</sub>Co<sub>1.5</sub>CrFeNi<sub>1.5</sub>Ti HEA at 1000 °C for 5h (C01).

<i>As-cast + Heat treated 1000 °C for 5h (C01)</i>	
<i>Crystal structure</i>	<i>Wt. %</i>
Ni (FCC)	67.1
Fe (BCC)	17.0
CrFe (Sigma)	2.8
Hexagonal C14-Fe <sub>2</sub> Ti (Laves)	10.5
Hexagonal D0 <sub>24</sub> -Ni <sub>3</sub> Ti	2.6

**Table 4** Phases present in the annealed sample of Al<sub>0.2</sub>Co<sub>1.5</sub>CrFeNi<sub>1.5</sub>Ti HEA at 1000 °C for 5h and subsequent treatment at 750 °C for additional 5h (C02).

<i>As-cast + Heat treated 1000 °C for 5h + 750 °C for 5h (C02)</i>	
<i>Crystal structure</i>	<i>Wt. %</i>
Ni (FCC)	48.2
Fe (BCC)	18.1
CrFe (Sigma)	5.9
Hexagonal C14-Fe <sub>2</sub> Ti (Laves)	25.4
Hexagonal D0 <sub>24</sub> -Ni <sub>3</sub> Ti	2.4

XRD analysis of the C01 and C02 showed the presence of the same phases in different amounts, with Hexagonal D0<sub>24</sub> in a very small amount, which probably precipitated during cooling. However, the amount of Laves phase was found to be significantly higher in comparison with C01. In short, XRD results reported increased stability of the FCC phase and decreased amount of the sigma phase as a ThermoCalc simulation predicted.

### 5.3 Microstructure evaluation

#### *As-cast alloy*

A scanning electron microscope was utilized to carry out the microstructural characterization of the as-cast sample and annealed samples (C01, C02). The micrographs comparison of as-cast and annealed Al<sub>0.2</sub>Co<sub>1.5</sub>CrFeNi<sub>1.5</sub>Ti HEAs are demonstrated in Fig. 13, Fig. 14, and Fig. 15. Metallographic maps of high entropy alloys exhibit the distribution of dendritic structures in the as-cast alloy. After annealing, the alloys still show the presence of remaining dendrites in certain areas, indicating that the heat treatment would need to be performed for longer times in order to fully dissolve the dendritic microstructure. Typical cast-dendrite morphology appears as dendritic structures separated by interdendritic areas, as shown in Fig. 13b. The arrows on the figure denote DR for dendritic regions and ID for interdendritic regions.

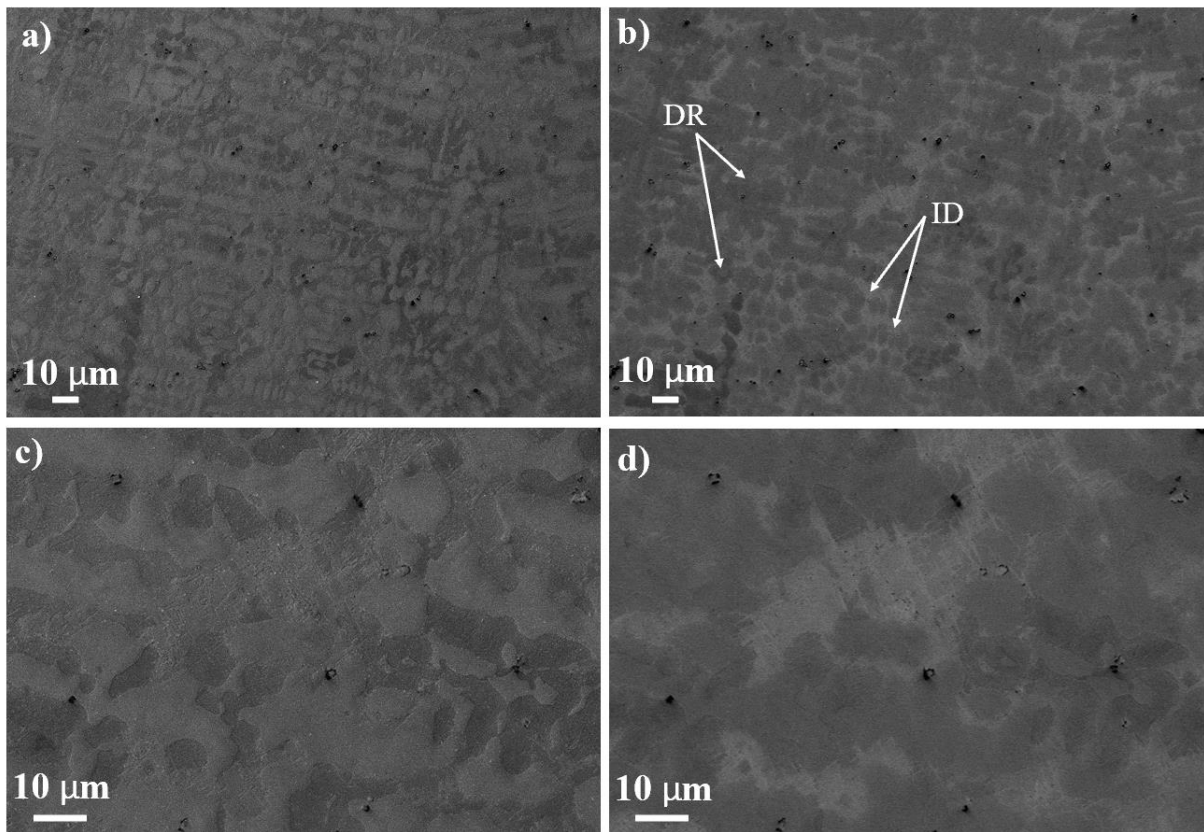


**Fig. 13** Scanning electron microscopic images of the morphology and microstructures of the as-cast sample of  $\text{Al}_{0.2}\text{Co}_{1.5}\text{CrFeNi}_{1.5}\text{Ti}$  high entropy alloy a) using secondary electrons (SE) detector; b) using backscattered electrons (BSE); c) amplified view of the microstructure using SE detector; d) amplified view of the microstructure using BSE detector.

The dark grey dendrite and light grey interdendritic regions visible on the backscattered (BSE) image are in contrast, which could be a reflection of different elementary segregation. The chemical composition of these areas for as-cast and annealed alloys was analyzed by EDS with the detailed discussion in the EDS analysis subchapter. The dendrite region was found to be rich in Ni, Co, and Al, while the interdendritic found to exhibit elemental enrichment of Cr and Fe [78].

#### ***Annealing at 1000 °C for 5h***

The as-cast  $\text{Al}_{0.2}\text{Co}_{1.5}\text{CrFeNi}_{1.5}\text{Ti}$  HEA was heat-treated at 1000 °C for 5h, labeled as C01, where the phase composition was characterized by XRD in Fig. 12. Similar to the as-cast alloy, the C01 sample exhibit still a few areas of dendritic structure, shown in Fig. 14b, despite the heat treatment. After annealing, a complex microstructure is revealed probably due to the diffusion of certain elements, and very small precipitates appear, which can be identified complementary by the XRD results. These precipitates were probably too small in size to be identified by the SEM micrographs on the as-cast state.

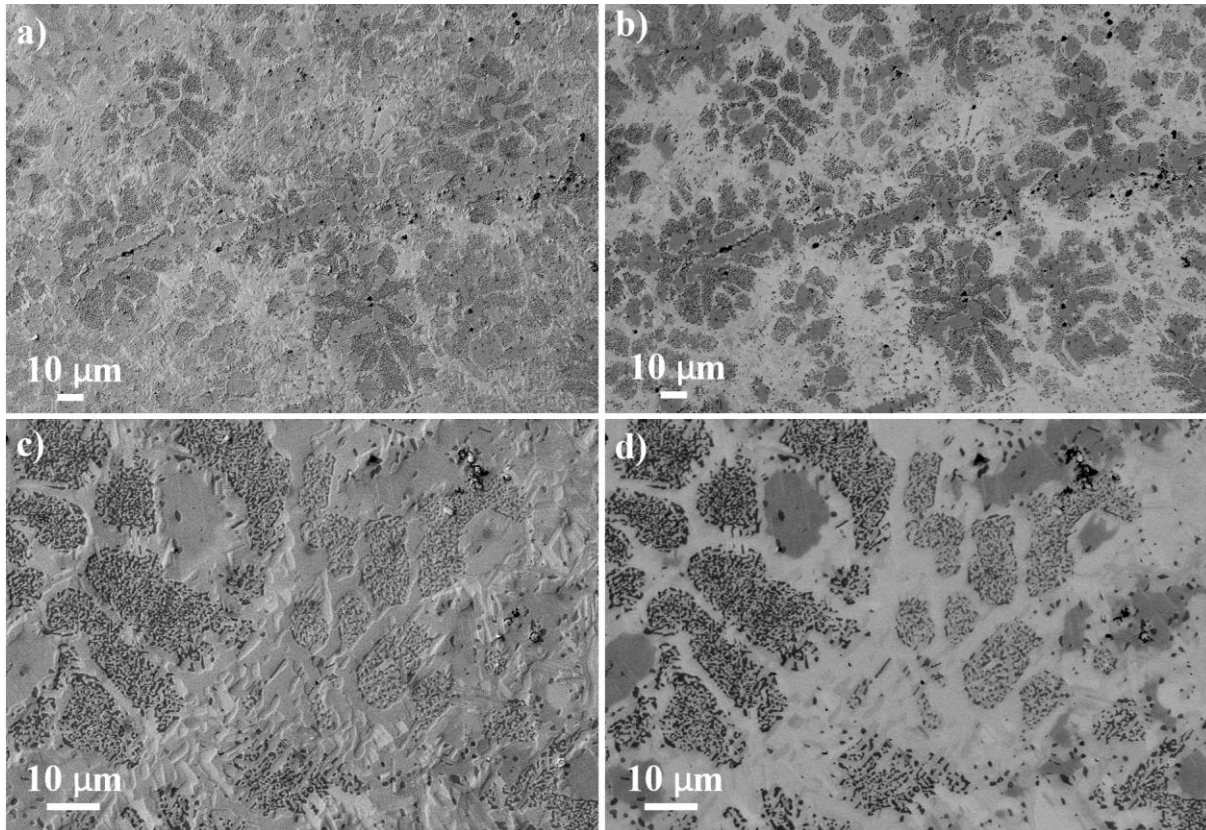


**Fig. 14** Scanning electron microscopic images of the morphology and microstructures of the annealed sample of  $\text{Al}_{0.2}\text{Co}_{1.5}\text{CrFeNi}_{1.5}\text{Ti}$  HEA at  $1000\text{ }^{\circ}\text{C}$  for 5h (C01) a) using secondary electrons (SE) detector; b) using backscattered electrons (BSE); c) amplified view of the microstructure using SE detector; d) amplified view of the microstructure using BSE detector.

The final comparison of the SEM and XRD results obtained during the present study with the calculated pseudo binary phase diagram by CALPHAD showed some differences. C01 should consist only of BCC and FCC phases as per the calculated phase diagram by CALPHAD. Although, XRD analysis confirmed the presence of FCC, BCC, Laves, sigma, and Hexagonal  $\text{DO}_{24}$  phases after the first heat treatment. It could be argued that 5 hours was not enough to dissolve each present phase, therefore not creating a microstructure composed of FCC and BCC only. However, it should be noted that ThermoCalc works with an ideal state of equilibrium. In this case, ideal conditions were not reached. In addition, for a better microstructural investigation, temperature optimization and deeper research are necessary.

#### ***Annealing at $1000\text{ }^{\circ}\text{C}$ for 5h with subsequent $750\text{ }^{\circ}\text{C}$ for additional 5h***

The  $\text{Al}_{0.2}\text{Co}_{1.5}\text{CrFeNi}_{1.5}\text{Ti}$  HEA was heat-treated at  $1000\text{ }^{\circ}\text{C}$  for 5h with a subsequent treatment at  $750\text{ }^{\circ}\text{C}$  for an additional 5h, labeled as C02. In the C02 sample also the dendritic structure is preserved in a few spots, as shown in Fig. 15b. However, the C02 sample also exhibits a very complex microstructure in terms of phase present, these could be identified by the different scales of grey color in the BSE image. Additionally, complementing the results with XRD is necessary in order to identify the additional phases.

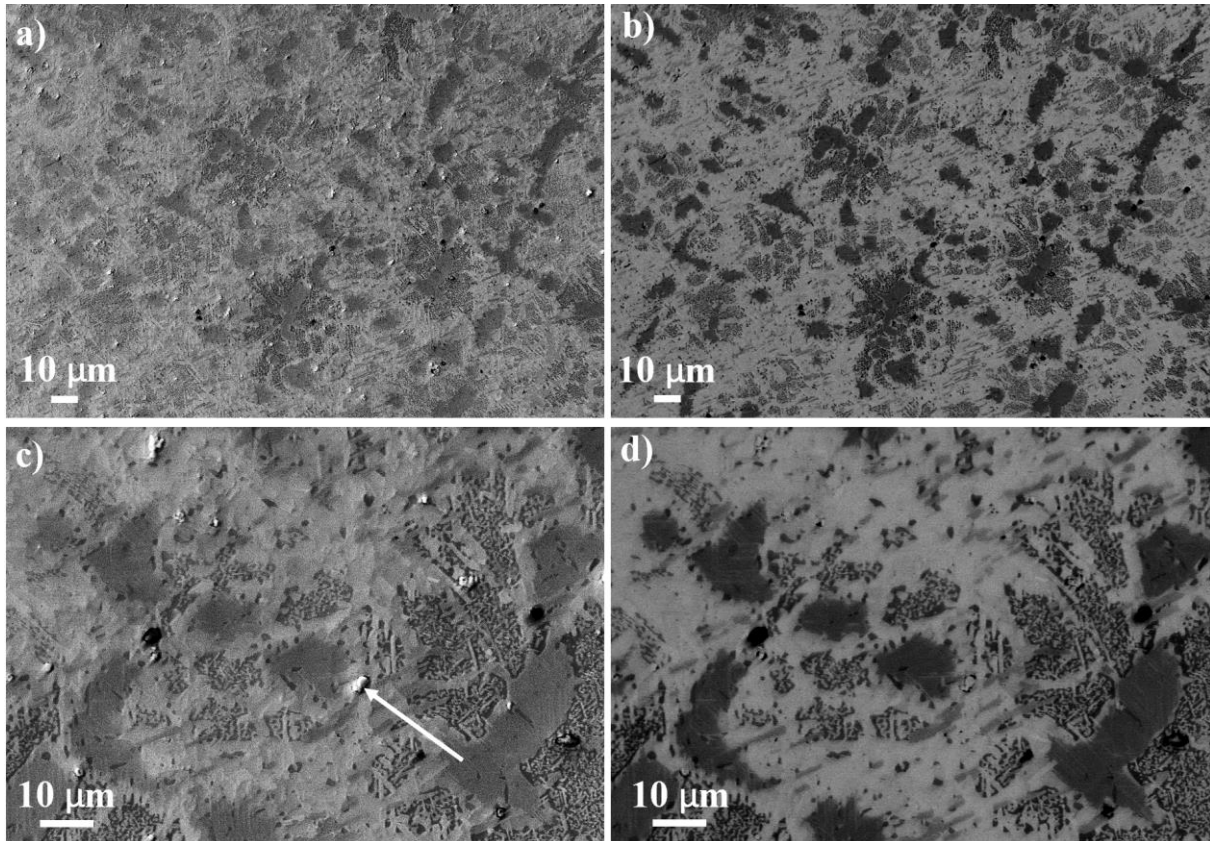


**Fig. 15** Scanning electron microscopic images of the morphology and microstructures of the annealed sample of  $\text{Al}_{0.2}\text{Co}_{1.5}\text{CrFeNi}_{1.5}\text{Ti}$  HEA at  $1000\text{ }^{\circ}\text{C}$  for 5h and subsequent treatment at  $750\text{ }^{\circ}\text{C}$  for additional 5h (C02) a) using secondary electrons (SE) detector; b) using backscattered electrons (BSE); c) amplified view of the microstructure using SE detector; d) amplified view of the microstructure using BSE detector.

In this case, a comparison of results from SEM and XRD with the calculated phase diagram was in good agreement. XRD analysis confirmed the presence of all phases predicted by ThermoCalc simulation, except Hexagonal  $\text{D0}_{24}$  that precipitates during cooling, as mentioned in the XRD analysis section. However, the Hexagonal  $\text{D0}_{24}$  is exposed in very small amounts and is difficult to define using SEM, in order to confirm and examine its occurrence, transmission electron microscopy (TEM) is required. Furthermore, the SEM results confirmed the presence of a small amount of oxides on this sample, marked with a white arrow in Fig. 15c. In contrast, the oxides were not detected in the XRD analysis since they are obtained only in a very small amount and their content might be below the detection threshold of the XRD method. The formation of oxides is a result of the long annealing rate in a furnace with an air atmosphere, approx. 10h. To prevent the formation of oxides a furnace with an inert atmosphere is necessary.

Another interesting aspect of the microstructure, both as-cast and annealed, is the morphology of the phases. The structure has not undergone recrystallization, since the original microstructure was not severely plastically deformed before heat treatments, but only cast. In conclusion, the microstructure seems to be thermally stable under experimental conditions in the range of annealing temperatures from  $750\text{ }^{\circ}\text{C}$  to  $1000\text{ }^{\circ}\text{C}$  for 5 hours, with subsequent treatment for additional 5 hours for the C02 sample.

## 5.4 EDS analysis

### *As-cast alloy*

In order to examine the chemical composition of the as-cast and annealed samples of  $\text{Al}_{0.2}\text{Co}_{1.5}\text{CrFeNi}_{1.5}\text{Ti}$  HEA, the energy dispersion spectroscopy (EDS) was performed. The average chemical composition of the as-cast  $\text{Al}_{0.2}\text{Co}_{1.5}\text{CrFeNi}_{1.5}\text{Ti}$  HEA was calculated by EDS area analysis, which is shown in Table 5. These data were chosen as representative due to the analysis of the EDS, which was taken on large areas of the as-cast sample. In conclusion, the composition is in agreement with the theoretical composition, listed in Table 1.

**Table 5** Average chemical composition of the as-cast sample of  $\text{Al}_{0.2}\text{Co}_{1.5}\text{CrFeNi}_{1.5}\text{Ti}$  high entropy alloy, obtained from Map Data 1.

<i>Name of alloy</i>	<i>Composition of the as-cast alloy (atomic percent)</i>					
	<i>Al</i>	<i>Co</i>	<i>Cr</i>	<i>Fe</i>	<i>Ni</i>	<i>Ti</i>
<i><math>\text{Al}_{0.2}\text{Co}_{1.5}\text{CrFeNi}_{1.5}\text{Ti}</math></i>	2.90	24.70	14.80	16.20	26.60	14.80

The microstructure of the alloy prior to the annealing treatment is shown in Fig. 16. EDS analysis of the total composition confirms the non-equiatomic proportion of the metals in the alloy, as listed in Table 5. The presented high entropy alloy in this study was characterized as an Al-poor alloy with a higher amount of Ni. In contrast to the fewer number of phases generally believed to be detected in HEAs, the as-cast alloy presented in this study was found to contain 4 different phases using XRD analysis. It should be noted that the phase identification has been performed by contrast and compositional differences.

Fig. 16 vividly shows large bright areas marked as region 1. It should be noted, that the composition for each region has been reported in atomic percent (at. %) throughout this study, where the additional mass fraction for the as-cast alloy is listed in Table 6, and for annealed alloys in Table 8 and Table 10. The EDS shows that region 1 is rich in similar amounts in Ni (25.5 %), Co (24.6 %), Fe (19.76 %), Cr (18.75 %) along with trace elements Ti (9.1 %) and Al (2.29 %). Region 2, exhibits elements with a similar amount of atomic percent in structure as region 1, where Ti (16.79 %), Fe (16.65 %), and Cr (16.8 %) is exposed in the equiatomic amount. This phenomenon could be due to the higher presence of the Laves and sigma phase in region 2, as confirmed by XRD results. The dark area, marked as region 3, is enriched with Ni (27.66 %), Co (24.94 %), and Al (6.35 %), indicates the presence of a dendritic region.

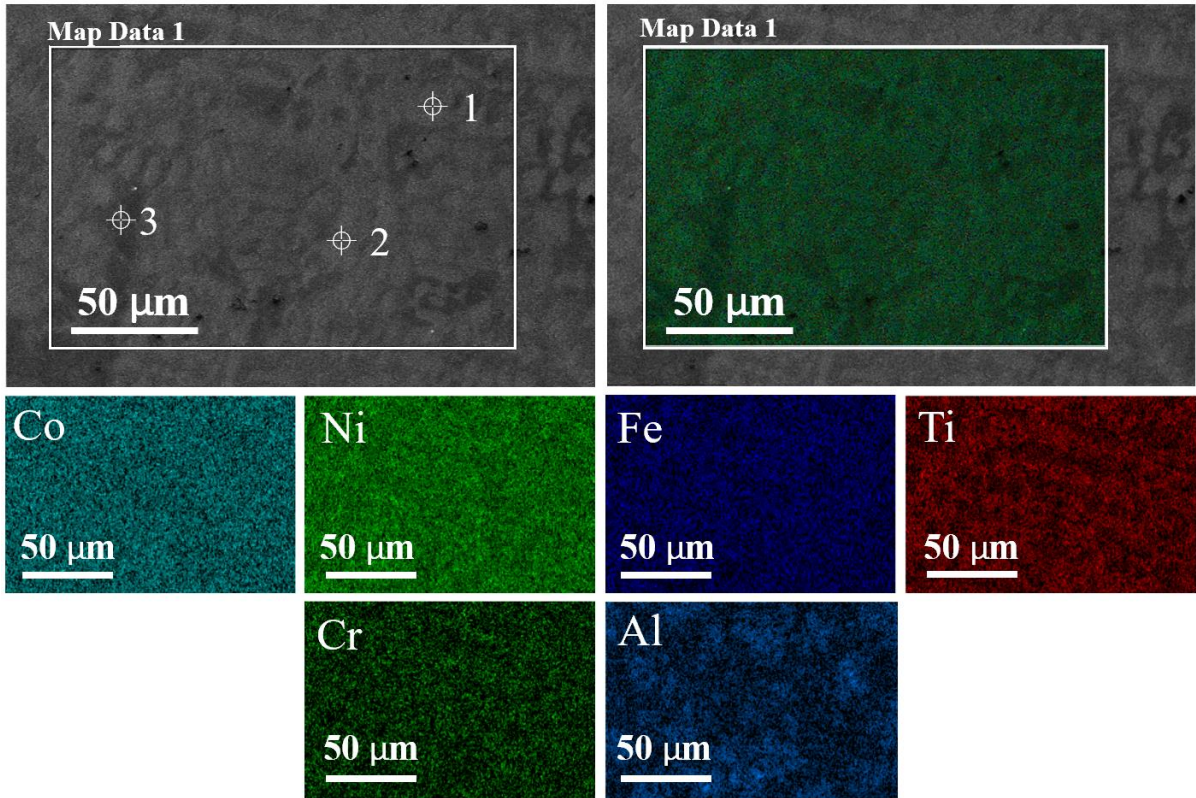


**Fig. 16** Microstructure and elements mapping by EDS of the as-cast sample of  $\text{Al}_{0.2}\text{Co}_{1.5}\text{CrFeNi}_{1.5}\text{Ti}$  high entropy alloy.

**Table 6** Chemical composition for presented regions of the as-cast sample of  $\text{Al}_{0.2}\text{Co}_{1.5}\text{CrFeNi}_{1.5}\text{Ti}$  high entropy alloy.

<i>Element</i>	<i>Region 1</i>		<i>Region 2</i>		<i>Region 3</i>	
	<i>Wt. %</i>	<i>Atomic %</i>	<i>Wt. %</i>	<i>Atomic %</i>	<i>Wt. %</i>	<i>Atomic %</i>
Al	1.12	2.29	0.48	0.98	3.19	6.35
Ti	7.89	9.10	14.62	16.79	15.98	17.87
Cr	17.65	18.75	15.87	16.80	10.21	10.55
Fe	19.98	19.76	16.90	16.65	13.12	12.63
Co	26.25	24.60	26.00	24.28	27.34	24.94
Ni	27.11	25.50	26.13	24.50	30.16	27.66

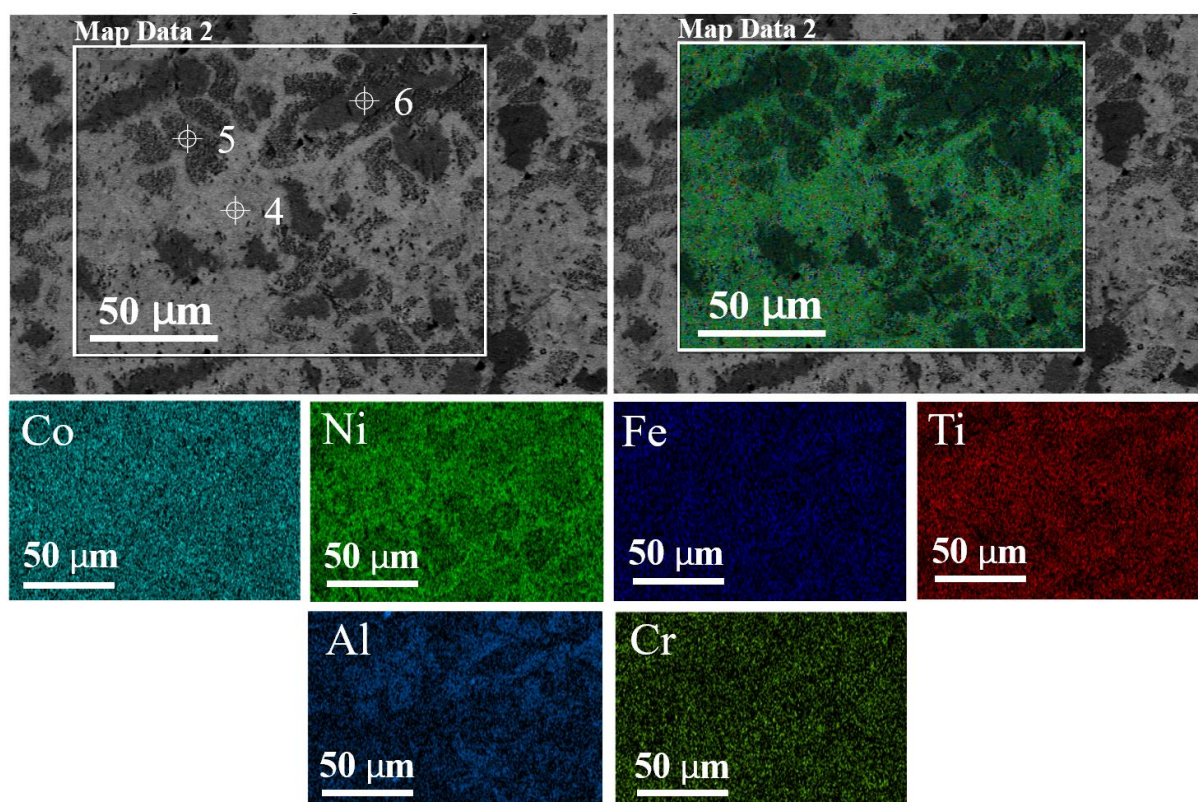
### **Annealing at 1000 °C for 5h**

Fig. 17 shows annealed microstructure at 1000 °C for 5 hours along with the EDS analysis indicating the locations of various elements and their approximate compositions, listed in Table 8. First, the non-equiatomic composition of the alloy has been verified by EDS as well, shown in Table 7.

**Table 7** Average chemical composition of the annealed sample of  $\text{Al}_{0.2}\text{Co}_{1.5}\text{CrFeNi}_{1.5}\text{Ti}$  HEA at 1000 °C for 5h (C01), obtained from Map Data 2.

Name of alloy	Composition of the C01 alloy (atomic percent)								
	Al	Co	Cr	Fe	Ni	Ti	Zr	Si	W
$\text{Al}_{0.2}\text{Co}_{1.5}\text{CrFeNi}_{1.5}\text{Ti}$	2.90	24.30	15.10	16.40	26.20	14.60	0.20	0.20	0.10

Ni is mostly present in region 4 and it contains 41.08 %Ni. It contains, approximately, 23.88 % and 18.85 % of Co and Ti (respectively) while other elements are present in minor amounts. The clouded area, marked as region 5 is Co (25.08 %), Ni (23.63 %), rich where an increased amount of Ti (14.34 %) and Fe (15.54 %) was detected, which might indicate, the occurrence of Laves phase [79]. It should be noted since the phases are very small in this particular area, there could be the influence of the elemental composition of neighboring regions. The EDS point analysis on this area was performed at higher magnifications in order to avoid the influence of the other considered elements, therefore the location of point 5 in Fig. 17 is representative. Region 6 is essentially Ni (24.87 %), Co (24.46 %), Fe (22.85 %), and Cr (18.13 %), rich, due to the possible presence of the sigma phase, as previously reported [80].



**Fig. 17** Microstructure and elements mapping by EDS of the annealed sample of  $\text{Al}_{0.2}\text{Co}_{1.5}\text{CrFeNi}_{1.5}\text{Ti}$  HEA at 1000 °C for 5h (C01).

**Table 8** Chemical composition for presented regions of the annealed sample of  $\text{Al}_{0.2}\text{Co}_{1.5}\text{CrFeNi}_{1.5}\text{Ti}$  HEA at 1000 °C for 5h (C01).

Element	Region 4		Region 5		Region 6	
	Wt. %	Atomic %	Wt. %	Atomic %	Wt. %	Atomic %
Al	0.48	1.00	2.53	5.07	0.73	1.50
Ti	16.19	18.85	15.22	17.14	7.06	8.19
Cr	5.28	5.66	13.05	13.54	16.98	18.13
Fe	9.55	9.54	16.09	15.54	22.98	22.85
Co	25.24	23.88	27.40	25.08	25.95	24.46
Ni	43.25	41.08	25.71	23.63	26.29	24.87

**Annealing at 1000 °C for 5h with subsequent 750 °C for additional 5h**

The microstructure of the  $\text{Al}_{0.2}\text{Co}_{1.5}\text{CrFeNi}_{1.5}\text{Ti}$  HEA developed during annealing at 1000 °C for 5h with subsequent 750 C for an additional 5h is shown in Fig. 18. The average chemical composition for the C02 sample is listed in Table 9, whereas the chemical composition for the presented regions is listed in Table 10.

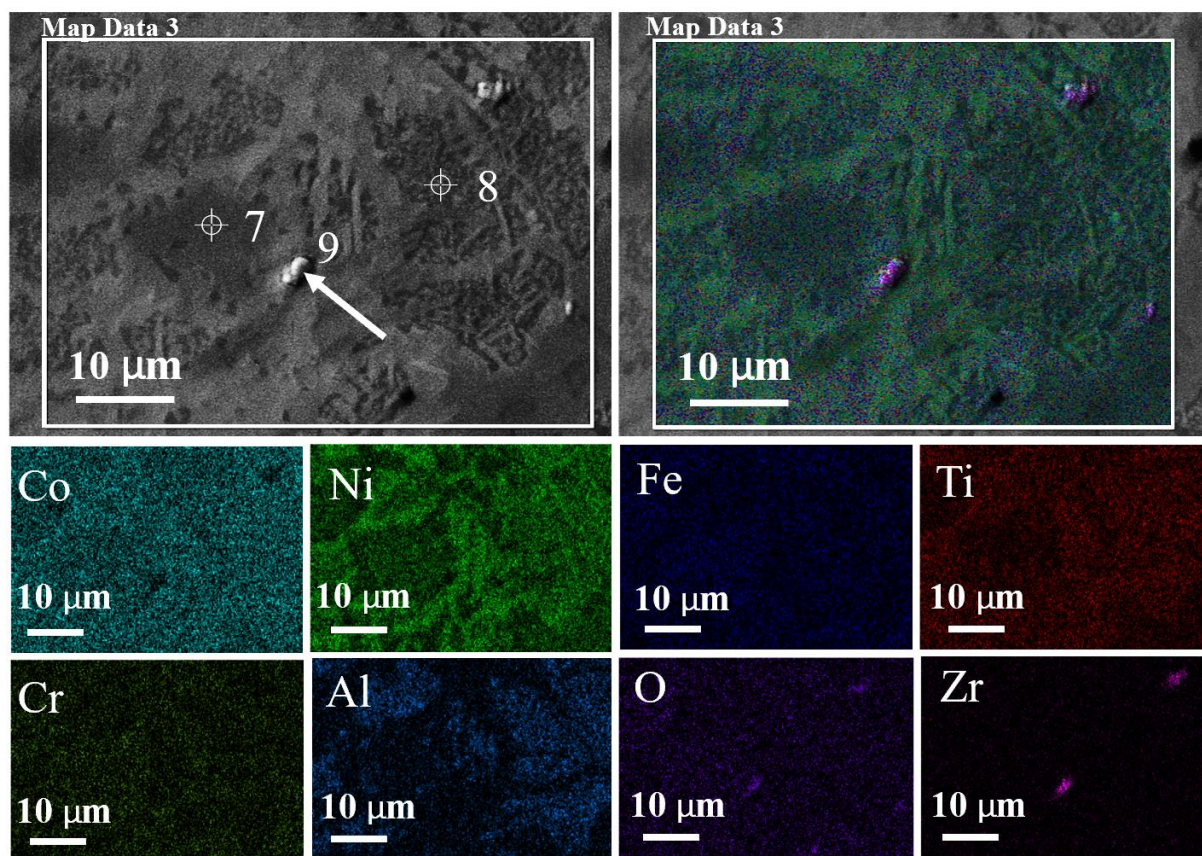


**Fig. 18** Microstructure and elements mapping by EDS of the annealed sample of  $\text{Al}_{0.2}\text{Co}_{1.5}\text{CrFeNi}_{1.5}\text{Ti}$  HEA at 1000 °C for 5h and subsequent treatment at 750 °C for additional 5h (C02).

**Table 9** Average chemical composition of the annealed sample of Al<sub>0.2</sub>Co<sub>1.5</sub>CrFeNi<sub>1.5</sub>Ti HEA at 1000 °C for 5h with subsequent 750 °C for additional 5h (C02), obtained from Map Data 3.

<i>Name of alloy</i>	<i>Composition of the C02 alloy (atomic percent)</i>							
	<i>Al</i>	<i>Co</i>	<i>Cr</i>	<i>Fe</i>	<i>Ni</i>	<i>Ti</i>	<i>Zr</i>	<i>Si</i>
<i>Al<sub>0.2</sub>Co<sub>1.5</sub>CrFeNi<sub>1.5</sub>Ti</i>	3.90	24.70	13.90	15.30	27.20	14.70	0.20	0.20

The EDS point analysis shows that region 7 is rich with elements such as Ni, Co, Fe, and Ti are all within a range of 18.21 % to 25.63 %. This could indicate the presence of the sigma phase in the interdendritic region [81]. Another, cloudy area, marked as region 8, is Ni (27.67 %) and Cr (26.56 %) rich along with Ti (19.07 %) and trace elements Cr (7.09 %) and (9.9 %). Region 9 is O (46.14 %) and Zr (27.09 %) rich, which is explained by the possible presence of oxides as a result of a long annealing time in a furnace with an air atmosphere. From the chemical composition of region 9, listed in Table 10, it can be determined that the oxide Zr-rich. The presence of trace elements of Si and Hf may be explained due to potential contamination of the furnace with the air atmosphere.

**Table 10** Chemical composition for presented regions of the annealed sample of Al<sub>0.2</sub>Co<sub>1.5</sub>CrFeNi<sub>1.5</sub>Ti HEA at 1000 °C for 5h and subsequent treatment at 750 °C for additional 5h (C02).

<i>Element</i>	<i>Region 7</i>		<i>Region 8</i>		<i>Region 9</i>	
	<i>Wt. %</i>	<i>Atomic %</i>	<i>Wt. %</i>	<i>Atomic %</i>	<i>Wt. %</i>	<i>Atomic %</i>
Al	0.59	1.22	5.06	9.90	0.25	0.43
Ti	7.12	8.27	17.31	19.07	8.41	8.23
Cr	17.03	18.21	6.99	7.09	3.75	3.38
Fe	23.83	23.71	10.12	9.56	4.05	3.41
Co	27.18	25.63	29.67	26.56	6.12	4.88
Ni	24.25	22.96	30.78	27.67	7.60	6.07
Zr	-	-	-	-	52.67	27.09
O	-	-	-	-	15.73	46.14
Si	-	-	0.07	0.14	-	-
Hf	-	-	-	-	1.41	0.37

## 5.5 Microhardness and nanoindentation hardness evaluation

To evaluate the effect of heat treatment on the mechanical properties of the studied system, micro Vickers hardness testing for as-cast and annealed samples (C01, C02) of Al<sub>0.2</sub>Co<sub>1.5</sub>CrFeNi<sub>1.5</sub>Ti HEA were carried out. Variation of microhardness of the as-cast and annealed (C01, C02) samples are shown in Fig. 19, where the average microhardness values in the Vickers scale are listed in Table 11. The average microhardness of the as-cast sample is 665±78 HV0.2, whereas the average microhardness of the heat-treated C01 and C02 samples is found to be 606±47 HV0.2, and 751±49 HV0.2.

**Table 11** Evaluation of microindentation test results for the as-cast and annealed samples (C01, C02) of  $\text{Al}_{0.2}\text{Co}_{1.5}\text{CrFeNi}_{1.5}\text{Ti}$  high entropy alloy.

<i>Indentation area</i>	<i>Average hardness value [HV 0.2]</i>	<i>Standard deviation [HV 0.2]</i>
As-cast	665	78
C01	606	47
C02	751	49

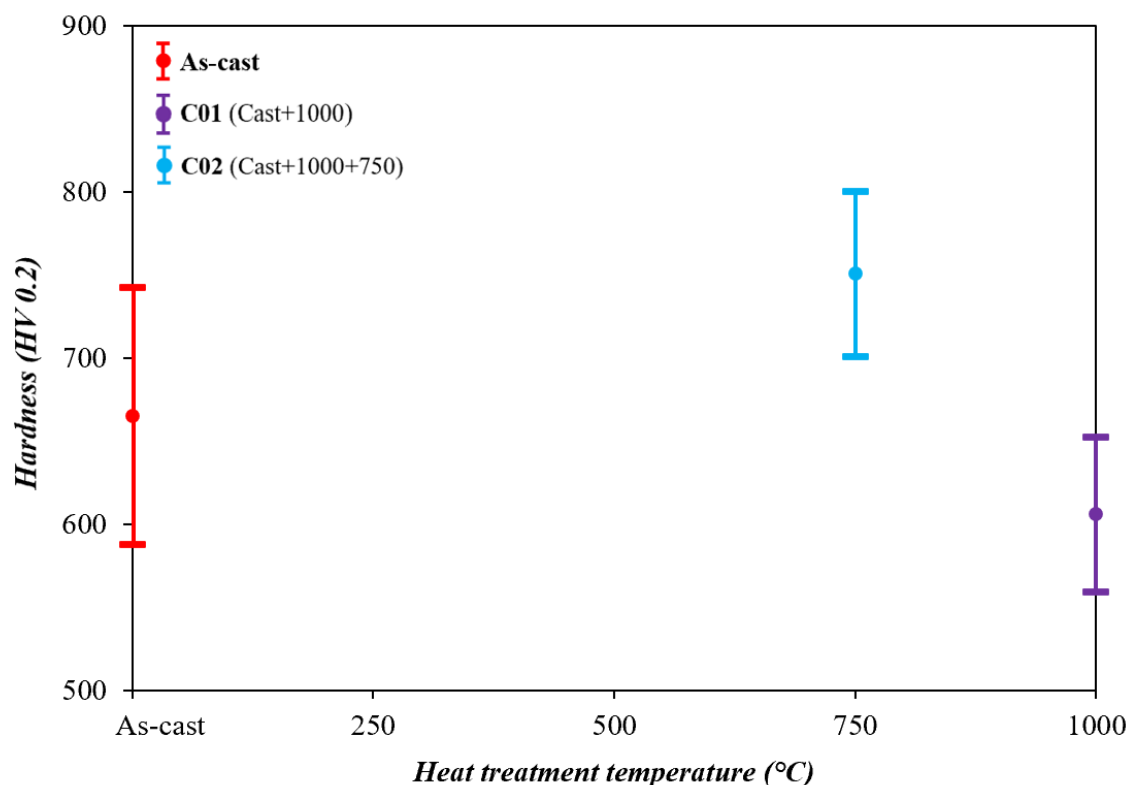


**Fig. 19** Microhardness of the  $\text{Al}_{0.2}\text{Co}_{1.5}\text{CrFeNi}_{1.5}\text{Ti}$  high entropy alloy in as-cast or annealed states (C01, C02).

The experimental results suggest that annealing at 1000 °C for 5h resulted in a probable slight decrease in hardness from the as-cast condition,  $665 \pm 78$  HV0.2 to  $606 \pm 47$  HV0.2, respectively. It could be explained by the fact that increasing the annealing temperature causes an increase in the volume fraction of the ductile FCC phase, which is responsible for the decrease in hardness [82]. In addition, grain growth at elevated temperatures may also contribute towards the decrease in hardness and directly impacts their performance [83]. On the other hand, the microhardness increased after annealing at 1000 °C for 5h followed by treatment at 750 °C for an additional 5h, indicating that a small amount of phases precipitated after this annealing, as shown by the XRD results. In addition, the presence of the sigma phase in a higher fraction than compared to the previous state has contributed to increasing the microhardness of the alloys more than the BCC phase, since the sigma phase is much harder [84]. With the increasing volume fraction of the sigma phase and Laves phase, the alloys become harder. Therefore, the

microhardness of the C02 sample reaches  $751\pm 49$  HV0.2, respectively, which is harder than (Al02Ti10) alloy (approx. 717 HV) in Ref. [72].

In addition, by analyzing the nanoindentation hardness and elastic modulus  $E$  of the as-cast sample, according to the Oliver-Pharr method, the nanoindentation tests were performed. Fig. 20 represents the morphology image of the studied alloy with assigned tip place for the dendritic region (Fig. 20a) and for the interdendritic region (Fig. 20b). The obtained values of nanohardness for light grey dendritic and dark grey interdendritic regions are listed in Table 12. The Young's modulus for dendritic and interdendritic regions are  $E_{\text{Dendritic}}=222\pm 11$  GPa and  $E_{\text{Interdendritic}}= 223\pm 50$  GPa, respectively. Both the study regions are distinctly different in nano hardness values,  $7234\pm 380$  MPa for DR region and,  $11760\pm 1089$  MPa for ID region, respectively, while the obtained values of Young's modulus are similar within their standard deviation. The increased value of the hardness in the ID region is due to the presence of a sigma and Laves phase, as was reported in Ref. [77]. The Young's modulus is comparable to the other high entropy alloys reported in the literature, like Al<sub>0.5</sub>CoCrFeNi, approx. 220 GPa [85].

**Table 12** Evaluation of nanoindentation results for the as-cast sample of Al<sub>0.2</sub>Co<sub>1.5</sub>CrFeNi<sub>1.5</sub>Ti high entropy alloy.

<i>Indentation area</i>	<i>Indentation hardness [MPa]</i>	<i>Average hardness value [HV]</i>	<i>Elastic modulus [GPa]</i>
DR	$7234\pm 380$	$669\pm 35$	$222\pm 11$
ID	$11760\pm 1089$	$1089\pm 47$	$223\pm 50$

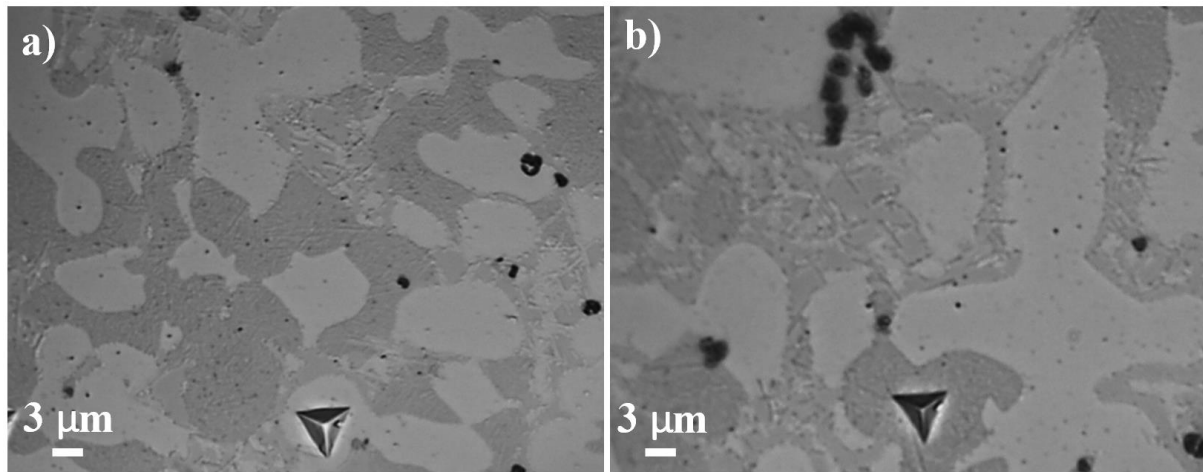


**Fig. 20** Scanning electron microscopic images of the morphology of the as-cast sample of Al<sub>0.2</sub>Co<sub>1.5</sub>CrFeNi<sub>1.5</sub>Ti high entropy alloy using secondary electrons (SE) detector, with assigned tip place for the a) dendritic region; b) interdendritic region.

## 6 Conclusions

In this study, the non-equiatomic  $\text{Al}_{0.2}\text{Co}_{1.5}\text{CrFeNi}_{1.5}\text{Ti}$  HEA produced by vacuum induction melting was characterized. The effect of heat treatments on microstructure, chemical composition, and mechanical properties of  $\text{Al}_{0.2}\text{Co}_{1.5}\text{CrFeNi}_{1.5}\text{Ti}$  HEA was investigated. The following was concluded:

1. The average chemical composition of  $\text{Al}_{0.2}\text{Co}_{1.5}\text{CrFeNi}_{1.5}\text{Ti}$  HEA was in good agreement with theoretical chemical composition, thus showing a successful production of the alloy by vacuum induction melting.
2. New Hexagonal  $\text{DO}_{24}$  phase was observed in the annealed states of  $\text{Al}_{0.2}\text{Co}_{1.5}\text{CrFeNi}_{1.5}\text{Ti}$  HEA, due to the possible precipitation during cooling. This phase was not detected in the as-cast state.
3. Temperature and time optimization of heat treatments and deeper research are necessary to confirm the phase composition predicted by ThermoCalc simulation.
4. Elemental segregation was detected both as-cast and annealed  $\text{Al}_{0.2}\text{Co}_{1.5}\text{CrFeNi}_{1.5}\text{Ti}$  HEAs, despite the applied heat treatments.
5. An increased microhardness value,  $751\pm 49$  HV0.2 was observed in the annealed C02 sample in comparison with annealed C01 sample, which showed a hardness of  $606\pm 47$  HV0.2. This may be explained by the higher amount of intermetallic phases on the former, which is in agreement with the ThermoCalc prediction.
6. The values of nanohardness for the dendritic and interdendritic regions for as-cast  $\text{Al}_{0.2}\text{Co}_{1.5}\text{CrFeNi}_{1.5}\text{Ti}$  HEA were distinctly different,  $7234\pm 380$  MPa for the DR region and,  $11760\pm 1089$  MPa for the ID region, respectively.
7. The obtained values of Young's modulus were similar within their standard deviation for the dendritic,  $222\pm 11$  GPa, and interdendritic,  $223\pm 50$  GPa, regions of the as-cast  $\text{Al}_{0.2}\text{Co}_{1.5}\text{CrFeNi}_{1.5}\text{Ti}$  HEA.

## Bibliography

- [1] GAO, Michael C., et al. High-entropy alloys. *Cham: Springer International Publishing*, 2016.
- [2] YEH, J.-W., et al. Nanostructured high-entropy alloys with multiple principal elements: novel alloy design concepts and outcomes. *Advanced Engineering Materials*, 2004, 6.5: 299-303.
- [3] MOGHADDAM, Ahmad Ostovari, et al. Additive manufacturing of high entropy alloys: a practical review. *Journal of Materials Science & Technology*, 2020.
- [4] BARRON, P. J., et al. Towards V-based high-entropy alloys for nuclear fusion applications. *Scripta Materialia*, 2020, 176: 12-16.
- [5] SENKOV, Oleg N., et al. Development and exploration of refractory high entropy alloys— A review. *Journal of materials research*, 2018, 33.19: 3092-3128.
- [6] FU, Xiaofeng; SCHUH, Christopher A.; OLIVETTI, Elsa A. Materials selection considerations for high entropy alloys. *Scripta Materialia*, 2017, 138: 145-150.
- [7] YANG, Xigang, et al. A novel, non-equiatomic NiCrWFeTi high-entropy alloy with exceptional phase stability. *Materials Letters*, 2020, 263: 127202.
- [8] NAIR, R. B., et al. Exceptionally high cavitation erosion and corrosion resistance of a high entropy alloy. *Ultrasonics sonochemistry*, 2018, 41: 252-260.
- [9] SHUANG, S., et al. Corrosion resistant nanostructured eutectic high entropy alloy. *Corrosion Science*, 2020, 164: 108315.
- [10] GORR, B., et al. Phase equilibria, microstructure, and high temperature oxidation resistance of novel refractory high-entropy alloys. *Journal of Alloys and Compounds*, 2015, 624: 270-278.
- [11] SHEN, Qingkai; KONG, Xiangdong; CHEN, Xizhang. Significant transitions of microstructure and mechanical properties in additively manufactured Al-Co-Cr-Fe-Ni high-entropy alloy under heat treatment. *Materials Science and Engineering: A*, 2021, 141257.
- [12] NIU, Sizhe, et al. Strengthening of nanoprecipitations in an annealed Al<sub>0.5</sub>CoCrFeNi high entropy alloy. *Materials Science and Engineering: A*, 2016, 671: 82-86.
- [13] XU, J., et al. Annealing-dependent microstructure, magnetic and mechanical properties of high-entropy FeCoNiAl<sub>0.5</sub> alloy. *Materials Science and Engineering: A*, 2020, 776: 139003.
- [14] MURTY, B. S., J. W. YEH and S. RANGANATHAN. High-Entropy Alloys, Elsevier, Butterworth-Heinemann, London, 2014.

- [15] CANTOR, Brian. Multicomponent and high entropy alloys. *Entropy*, 2014, 16.9: 4749-4768.
- [16] CANTOR, Brain, et al. Microstructural development in equiatomic multicomponent alloys. *Materials Science and Engineering: A*, 2004, 375: 213-218.
- [17] OTTO, Frederik, et al. Decomposition of the single-phase high-entropy alloy CrMnFeCoNi after prolonged anneals at intermediate temperatures. *Acta Materialia*, 2016, 112: 40-52.
- [18] GEORGE, Easo P.; RAABE, Dierk; RITCHIE, Robert O. High-entropy alloys. *Nature Reviews Materials*, 2019, 4.8: 515-534.
- [19] DING, Jun, et al. Tunable stacking fault energies by tailoring local chemical order in CrCoNi medium-entropy alloys. *Proceedings of the National Academy of Sciences*, 2018, 115.36: 8919-8924.
- [20] MA, Duancheng, et al. Ab initio thermodynamics of the CoCrFeMnNi high entropy alloy: Importance of entropy contributions beyond the configurational one. *Acta Materialia*, 2015, 100: 90-97.
- [21] ZHANG, Fei, et al. Polymorphism in a high-entropy alloy. *Nature communications*, 2017, 8.1: 1-7.
- [22] HUANG, Kuo-Hsiung; YEH, J. W. A study on the multicomponent alloy systems containing equal-mole elements. *Hsinchu: National Tsing Hua University*, 1996, 1.
- [23] SHARMA, Piyush; DWIVEDI, V. K.; DWIVEDI, Shashi Prakash. Development of high entropy alloys: A review. *Materials Today: Proceedings*, 2021.
- [24] JENÍČEK, V.; DIBLÍKOVÁ, L.; BLÁHOVÁ, M. Electrochemical deposition of coatings of highly entropic alloys from non-aqueous solutions. *Koroze a ochrana materialu*, 2016, 60.1: 6-12.
- [25] YEH, Jien-Wei. Alloy design strategies and future trends in high-entropy alloys. *Jom*, 2013, 65.12: 1759-1771.
- [26] ZHANG, Yong. *High-Entropy Materials*. Singapore: Springer Nature Singapore Pte Ltd, 2019.
- [27] YEH, Jien-Wei. Physical metallurgy of high-entropy alloys. *Jom*, 2015, 67.10: 2254-2261.
- [28] FU, Yu, et al. Recent advances on environmental corrosion behavior and mechanism of high-entropy alloys. *Journal of Materials Science & Technology*, 2020.
- [29] MIRACLE, Daniel B.; SENKOV, Oleg N. A critical review of high entropy alloys and related concepts. *Acta Materialia*, 2017, 122: 448-511.

- [30] LU, Z. P., et al. An assessment on the future development of high-entropy alloys: Summary from a recent workshop. *Intermetallics*, 2015, 66: 67-76.
- [31] JIEN-WEI, Y. E. H. Recent progress in high entropy alloys. *Ann. Chim. Sci. Mat*, 2006, 31.6: 633-648.
- [32] WANG, Zhijun, et al. Atomic-size effect and solid solubility of multicomponent alloys. *Scripta Materialia*, 2015, 94: 28-31.
- [33] CHEN, Jian, et al. A review on fundamental of high entropy alloys with promising high-temperature properties. *Journal of Alloys and Compounds*, 2018, 760: 15-30.
- [34] HUME-ROTHERY, William. The structure of metals and alloys. *Indian Journal of Physics*, 1969, 11: 74-74.
- [35] WANG, Zhijun; GUO, Sheng; LIU, Chain Tsuan. Phase selection in high-entropy alloys: from nonequilibrium to equilibrium. *Jom*, 2014, 66.10: 1966-1972.
- [36] ZHANG, Yong, et al. Solid-solution phase formation rules for multi-component alloys. *Advanced Engineering Materials*, 2008, 10.6: 534-538.
- [37] YANG, X.; ZHANG, Yong. Prediction of high-entropy stabilized solid-solution in multi-component alloys. *Materials Chemistry and Physics*, 2012, 132.2-3: 233-238.
- [38] GUO, Sheng, et al. Effect of valence electron concentration on stability of fcc or bcc phase in high entropy alloys. *Journal of applied physics*, 2011, 109.10: 103505.
- [39] SCHUH, B., et al. Mechanical properties, microstructure and thermal stability of a nanocrystalline CoCrFeMnNi high-entropy alloy after severe plastic deformation. *Acta Materialia*, 2015, 96: 258-268.
- [40] STEPANOV, N. D., et al. Aging behavior of the HfNbTaTiZr high entropy alloy. *Materials 21Letters*, 2018, 211: 87-90.
- [41] CHANG, Hui-Wen, et al. Influence of substrate bias, deposition temperature and post-deposition annealing on the structure and properties of multi-principal-component (AlCrMoSiTi) N coatings. *Surface and Coatings Technology*, 2008, 202.14: 3360-3366.
- [42] TSAI, Ming-Hung; YEH, Jien-Wei; GAN, Jon-Yiew. Diffusion barrier properties of AlMoNbSiTaTiVZr high-entropy alloy layer between copper and silicon. *Thin Solid Films*, 2008, 516.16: 5527-5530.
- [43] TSAI, K.-Y.; TSAI, M.-H.; YEH, J.-W. Sluggish diffusion in Co-Cr-Fe-Mn-Ni high-entropy alloys. *Acta Materialia*, 2013, 61.13: 4887-4897.
- [44] PICKERING, E. J.; JONES, N. G. High-entropy alloys: a critical assessment of their founding principles and future prospects. *International Materials Reviews*, 2016, 61.3: 183-202.

- [45] ZOU, Yu, et al. Size-dependent plasticity in an Nb<sub>25</sub>Mo<sub>25</sub>Ta<sub>25</sub>W<sub>25</sub> refractory high-entropy alloy. *Acta Materialia*, 2014, 65: 85-97.
- [46] LI, Weidong, et al. Mechanical behavior of high-entropy alloys. *Progress in Materials Science*, 2021, 100777.
- [47] RANGANATHAN, S. Personal Communication, 2015.
- [48] ZHANG, Weiran; LIAW, Peter K.; ZHANG, Yong. Science and technology in high-entropy alloys. *Science China Materials*, 2018, 61.1: 2-22.
- [49] ZHANG, Yong; XING, Qiuwei. High Entropy Alloys: Manufacturing Routes. 2020.
- [50] ZHANG, Yong; LI, Ruixuan. New Advances in High-Entropy Alloys. 2020.
- [51] CHEN, Shuying; TONG, Yang; LIAW, Peter K. Additive manufacturing of high-entropy alloys: a review. *Entropy*, 2018, 20.12: 937.
- [52] ZHUANG, Yan-Xin; ZHANG, Xiu-Lan; GU, Xian-Yu. Effect of Annealing on Microstructure and Mechanical Properties of Al<sub>0.5</sub>CoCrFeMoxNi High-Entropy Alloys. *Entropy*, 2018, 20.11: 812.
- [53] SATHIYAMOORTHY, Praveen, et al. Effect of annealing on microstructure and tensile behavior of CoCrNi medium entropy alloy processed by high-pressure torsion. *Entropy*, 2018, 20.11: 849.
- [54] ZHANG, Fei, et al. High-pressure induced phase transitions in high-entropy alloys: A review. *Entropy*, 2019, 21.3: 239.
- [55] GUO, Jing, et al. Welding of high entropy alloys—A review. *Entropy*, 2019, 21.4: 431.
- [56] ŠENBERGER, Jaroslav, et al. Metallurgy cast steel. 2008.
- [57] ZHANG, Yong, et al. Fabrication routes. *High-Entropy Alloys*, 2016, 151-179
- [58] SINGH, Sheela, et al. Effect of decomposition of the Cr–Fe–Co rich phase of AlCoCrCuFeNi high entropy alloy on magnetic properties. *Ultramicroscopy*, 2011, 111.6: 619-622.
- [59] TUNG, Chung-Chin, et al. On the elemental effect of AlCoCrCuFeNi high-entropy alloy system. *Materials letters*, 2007, 61.1: 1-5.
- [60] WANG, Xiao, et al. Effect of Ti, Al and Cu addition on structural evolution and phase constitution of FeCoNi system equimolar alloys. In: *Materials Science Forum*. Trans Tech Publications Ltd, 2012. p. 335-338.
- [61] CHEN, Yu-Liang, et al. Competition between elements during mechanical alloying in an octonary multi-principal-element alloy system. *Journal of alloys and compounds*, 2009, 481.1-2: 768-775.

- [62] SRIHARITHA, R.; MURTY, B. S.; KOTTADA, Ravi S. Phase formation in mechanically alloyed  $\text{Al}_x\text{CoCrCuFeNi}$  ( $x = 0.45, 1, 2.5, 5$  mol) high entropy alloys. *Intermetallics*, 2013, 32: 119-126.
- [63] HAN, Bin, et al. Elemental phase partitioning in the  $\gamma$ - $\gamma'$   $\text{Ni}_2\text{CoFeCrNb}$  15 high entropy alloy. *Entropy*, 2018, 20.12: 910.
- [64] TSAU, Chun-Huei; TSAI, Meng-Chi. The effects of Mo and Nb on the microstructures and properties of  $\text{CrFeCoNi}$  (Nb, Mo) alloys. *Entropy*, 2018, 20.9: 648.
- [65] WANG, Wenrui, et al. Effect of molybdenum additives on corrosion behavior of  $(\text{CoCrFeNi})_{100-x}\text{Mox}$  high-entropy alloys. *Entropy*, 2018, 20.12: 908.
- [66] ZHANG, Hongling, et al. Effect of Zr addition on the microstructure and mechanical properties of  $\text{CoCrFeNiMn}$  high-entropy alloy synthesized by spark plasma sintering. *Entropy*, 2018, 20.11: 810.
- [67] SUN, Yuchen, et al. Phases, Microstructures and Mechanical Properties of  $\text{CoCrNiCuZn}$  High-Entropy Alloy Prepared by Mechanical Alloying and Spark Plasma Sintering. *Entropy*, 2019, 21.2: 122.
- [68] ZHANG, Yong, et al. Effects of nitrogen content on the structure and mechanical properties of  $(\text{Al}_{0.5}\text{CrFeNiTi}_{0.25})\text{N}_x$  high-entropy films by reactive sputtering. *Entropy*, 2018, 20.9: 624.
- [69] WANG, Qing, et al. Coherent precipitation and strengthening in compositionally complex alloys: a review. *Entropy*, 2018, 20.11: 878.
- [70] ZÝKA, Jiří, et al. Microstructure and room temperature mechanical properties of different 3 and 4 element medium entropy alloys from  $\text{HfNbTaTiZr}$  system. *Entropy*, 2019, 21.2: 114.
- [71] TSENG, Ko-Kai, et al. Effects of Mo, Nb, Ta, Ti, and Zr on Mechanical Properties of Equiatomic  $\text{Hf-Mo-Nb-Ta-Ti-Zr}$  Alloys. *Entropy*, 2019, 21.1: 15.
- [72] CHUANG, Ming-Hao, et al. Microstructure and wear behavior of  $\text{Al}_x\text{Co}_{1.5}\text{CrFeNi}_{1.5}\text{Ti}_y$  high-entropy alloys. *Acta Materialia*, 2011, 59.16: 6308-6317.
- [73] OLIVER, Warren Carl; PHARR, George Mathews. An improved technique for determining hardness and elastic modulus using load and displacement sensing indentation experiments. *Journal of materials research*, 1992, 7.6: 1564-1583.
- [74] ANDERSSON, Jan-Olof, et al. Thermo-Calc & DICTRA, computational tools for materials science. *Calphad*, 2002, 26.2: 273-312.
- [75] MAO, Huahai; CHEN, Hai-Lin; CHEN, Qing. TCHEA1: A thermodynamic database not limited for “high entropy” alloys. *Journal of Phase Equilibria and Diffusion*, 2017, 38.4: 353-368.

- [76] CHEN, Hai-Lin; MAO, Huahai; CHEN, Qing. Database development and Calphad calculations for high entropy alloys: Challenges, strategies, and tips. *Materials Chemistry and Physics*, 2018, 210: 279-290.
- [77] MORAVCIKOVA-GOUVEA, Larissa, et al. High-strength Al<sub>0.2</sub>Co<sub>1.5</sub>CrFeNi<sub>1.5</sub>Ti high-entropy alloy produced by powder metallurgy and casting: A comparison of microstructures, mechanical and tribological properties. *Materials Characterization*, 2020, 159: 110046.
- [78] MUNITZ, A., et al. Heat treatment impacts the micro-structure and mechanical properties of AlCoCrFeNi high entropy alloy. *Journal of Alloys and Compounds*, 2016, 683: 221-230.
- [79] CUI, Peng, et al. Effect of Ti on microstructures and mechanical properties of high entropy alloys based on CoFeMnNi system. *Materials Science and Engineering: A*, 2018, 737: 198-204.
- [80] ROGAL, Łukasz, et al. Microstructure and mechanical properties of Al–Co–Cr–Fe–Ni base high entropy alloys obtained using powder metallurgy. *Metals and Materials International*, 2019, 25.4: 930-945.
- [81] TSAI, Ming-Hung, et al. A second criterion for sigma phase formation in high-entropy alloys. *Materials Research Letters*, 2016, 4.2: 90-95.
- [82] SHABANI, Ali, et al. Evaluation of the mechanical properties of the heat treated FeCrCuMnNi high entropy alloy. *Materials Chemistry and Physics*, 2019, 221: 68-77.
- [83] VAIDYA, M., et al. Grain growth kinetics in CoCrFeNi and CoCrFeMnNi high entropy alloys processed by spark plasma sintering. *Journal of Alloys and Compounds*, 2019, 791: 1114-1121.
- [84] ZHU, Z. G., et al. Annealing effect on the phase stability and mechanical properties of (FeNiCrMn)<sub>(100-x)</sub>Co<sub>x</sub> high entropy alloys. *Journal of Alloys and Compounds*, 2017, 695: 2945-2950.
- [85] JIAO, Z. M., et al. Nanoindentation characterised plastic deformation of a Al<sub>0.5</sub>CoCrFeNi high entropy alloy. *Materials Science and Technology*, 2015, 31.10: 1244-1249.

## List of abbreviations

BCC	Body Centered Cubic
BSE	Backscattered Electrons
CALPHAD	Calculation of Phase Diagrams
DFT	Density-Functional Theory
DR	Dendritic Region
EBSD	Electron Backscatter Diffraction
EDS	Energy-Dispersive X-ray Spectroscopy
FCC	Face Centered Cubic
FFT	Fast-Fourier Transform
HCP	Hexagonal Close Packed
HEA	High Entropy Alloy
ID	Interdendritic Region
ISVP	Medium Frequency Vacuum Furnace
MA	Mechanical Alloying
OP-S	Standart furmed silica suspension for final polishing
SD	Spinodal Decomposition
SE	Secondary Electrons
SEM	Secondary Electron Microscope
TEM	Transmission Electron Microscope
VEC	Valence Electron Concetration
XRD	X-ray Diffraction